Fine Structure of Cloud Droplet Concentration as Seen from the Fast-FSSP Measurements. Part I: Method of Analysis and Preliminary Results

M. PINSKY AND A. P. KHAIN

The Institute of Earth Sciences, The Hebrew University of Jerusalem, Jerusalem, Israel

(Manuscript received 14 July 1999, in final form 2 January 2001)

ABSTRACT

A statistical analysis of a series of droplet arrival times measured by the Fast Forward-Scattering Spectrometer Probe (FSSP) during aircraft flights in cumulus clouds was conducted. The main purpose of the analysis was to determine whether droplet concentration fluctuates at small scales on the order of a few centimeters or whether these fluctuations are negligible as compared with the mean concentration.

In the analysis, the series of droplet arrival times is regarded as a generalized Poisson random process with time-dependent (or space dependent) parameters. The method developed is based on the representation of droplet concentration in a cloud along the aircraft track as the sum of three components: average droplet concentration in a cloud, large-scale fluctuations of droplet concentrations described by the Fourier series, and a small-scale noncoherent fraction of concentration fluctuation characterized by the energy spectrum and the correlation function. The efficiency of the method to estimate the amplitude and spatial characteristics of small-scale droplet concentration fluctuations and to calculate the profile of large-scale components of droplet concentration along the aircraft track was carefully tested using model-simulated series of droplet arrival times.

The method was used to analyze a measurement sample in a cumulus cloud on a 350-m segment. The properties of droplet concentration were calculated both over the whole cloud traverse and within the adiabatic core.

The results of the calculations show the existence of pronounced small-scale droplet concentration fluctuations in the case study. The rms of small-scale droplet concentration fluctuations was estimated to be about 31% of the mean values of droplet concentration both over the whole cloud and in a more homogeneous adiabatic core. The power spectrum shows that fluctuations with spatial scales within the 0.5–5-cm range contain over 80% of the energy of small-scale fluctuations.

1. Introduction

Several theoretical studies (e.g., Maxey 1987; Elperin et al. 1996; Pinsky and Khain 1996, 1997; Pinsky et al. 1999a), direct numerical simulations (Wang and Maxey 1993; Zhou et al. 1998), and laboratory experiments in wind channels (Fessler et al. 1994) indicate the existence of significant concentration inhomogeneities of inertial particles in a turbulent medium caused by their inertia. Pinsky and Khain (1997) and Pinsky et al. (1999a) theoretically investigated some characteristics of the fine structure of droplet concentration developing in a turbulent flow with the intensity of turbulence typical of cumulus clouds. They showed that because of drop inertia, the drop flux tended to be divergent even in a nondivergent turbulent flow. The drop flux divergence turned out to be maximum for 100-μm radii drops. Drops of smaller radii follow the air track of a nondivergent flow more closely. The sensitivity of drops of larger size to air velocity fluctuations is lower, so that gravity induced fall velocity dominates. Thus, the rate of concentration inhomogeneity was found to be greatly dependent on the drop size. Inhomogeneities of drop concentration were most pronounced for drops of 100-μm radii. However, drop flux divergence for small cloud droplets (10–15-μm radii) was found intense enough to provide significant drop concentration fluctuations reaching 20% to 40% of the mean drop concentration. The divergence of drop flux velocity for small cloud droplets was found to be proportional to the dissipation rate and to the square of the droplet radius (Pinsky et al. 1999a). They showed that the characteristic spatial scale of these fluctuations of droplet concentration is equal to one or a few centimeters: hence, clouds have a fine structure (''inch clouds'').

In case such centimeter-scale fluctuations were found in situ cloud observations, it would serve as an important evidence of effects of the drop inertia on droplet motion and interaction, predicted in theoretical studies (e.g., Pinsky et al. 1999a). The existence of droplet (and ice particles) concentration inhomogeneities at small scales can, in fact, be important for processes of droplet spectrum formation by diffusion and coalescence

Corresponding author address: Dr. Alexander P. Khain, The Ring Family Department of Atmospheric Sciences, The Institute of Earth Sciences, The Hebrew University of Jerusalem, Givat Ram, Jerusalem 91904 Israel.
E-mail: khain@ums.huji.ac.il

growth (e.g., Shaw et al. 1998; Zhou et al. 1998; Pinsky et al. 1997, 1999a,b, 2000; see also the discussion in appendix D).

Note that the problem of the existence of small-scale concentration fluctuations in clouds (the so-called preferential concentration) and their possible effects still remain a controversial issue in the cloud-physics community [see the comment of Grabowski and Vaillancourt (1999) on the paper by Shaw et al. (1998)]. That is why revealing spatial small-scale concentration inhomogeneities in clouds is an essential problem in cloud physics.

There are quite few experimental studies of the fine-scale structure of droplet fields in cumulus clouds. To examine the statistics of the droplet counting process, Baker (1992) used data from a Forward-Scattering Spectrometer Probe (FSSP)-100 recorded with the Particle Spacing Monitor (Baumgardner 1986). He found that the statistics over cumulus cloud sections showed significant deviations from the Poisson distribution, which characterizes a pure random spatial distribution of the droplets. In contrast, Chaumat and Brenguier (1998) used the data collected with the Fast FSSP (FFSSP; Brenguier et al. 1998) to document the same statistics in adiabatic (undiluted) cloud regions with narrow droplet spectra. They found that the statistics in those regions was close to the Poisson statistics, down to scales of a few millimeters.

We present here a method of statistical analysis of series of droplet arrival times measured with the FFSSP. The main purpose of the analysis is to determine whether droplet concentration fluctuates at scales as small as a few centimeters or if these fluctuations are negligible as compared to the mean concentration.

A series of droplet arrival times is regarded as a generalized Poisson random process with time-dependent (or space dependent) parameters. The method developed is based on the representation of droplet concentration in a cloud along the aircraft track as the sum of three components: average droplet concentration in the cloud section, large-scale fluctuations of droplet concentration described by the Fourier series, and a small-scale noncoherent fraction of concentration fluctuations characterized by the energy spectrum and the correlation function.

The paper has the following structure. Section 2 presents basic notions concerning the definition of droplet concentration in clouds and the connection of droplet concentration fluctuations with the Poisson random processes. The approach used to describe droplet concentration in clouds is presented in section 3. The relationship between the components of droplet concentration fluctuations and cloud section averaged parameters is analyzed in section 4. We present the statistical estimation and evaluation of errors in the droplet concentration parameters in section 5. Section 6 is devoted to tests of the algorithm. We present the results of the analysis of a series of droplet arrival times measured in situ in a cumulus cloud in section 7. The discussion and conclusions are presented in sections 8 and 9, respectively. Some mathematical derivations, as well as the discussion of possible effects of small-scale drop concentration inhomogeneities on the droplet size spectra are presented in appendices.

2. Basic notions

a. Droplet concentration

During aircraft flight in a cloud the FFSSP laser beam sweeps some air volume that contains droplets. When droplets cross the laser beam, they are registered by a photodetector and droplet arrival times are measured. As a result, an impulse process is formed at the photodetector output. Droplets are randomly distributed in space, and their counting with an airborne instrument generates a random series of counts. The sequence of time periods between droplet detections τ_i describes the spatial location of the droplets along the aircraft track. Using additional information about the aircraft velocity V and the cross section S of the laser beam perpendicular to the track, we can estimate droplet concentration and its variations along the track. The concentration can be estimated as

$$\hat{\lambda} = n \Big/ \left(SV \sum_i \tau_i \right), \tag{2.1}$$

where n is the number of droplets counted during the time period $\Sigma_i \tau_i$, and symbol $\hat{}$ indicates that the corresponding value is an estimation.

In fact, droplet concentration in an actual cloud is not uniform and droplet measurements aim at describing its variability, in relation with air velocity, temperature, and so on. If the spatial resolution of measurements is such that the number of counts in each sample is large, (2.1) will provide a good estimation of droplet concentration, that is, $\hat{\lambda} \to \lambda$, when $n \to \infty$.

A problem arises when processing the data at a very fine spatial resolution. Taking into account the discrete nature of the droplet field, the number of counts within segment l, as l tends to 0, would be equal either to 0 or to 1. Therefore, according to (2.1), the estimation of the concentration would be either 0 or infinity.

To retrieve the expected value of counts over a short segment, the measurements should be repeated many times, which is not possible with an aircraft in the atmosphere. Thus, the problem is to get the best description of the variability of droplet concentration at the finest possible scale, from a single realization of the counting process.

We will use the definition of droplet concentration given by Pawlowska and Brenguier (1997) as the expectation of the number of droplets per volume $V = Sl$, when V tends to 0:

$$\lambda = \left\langle \lim_{l \to 0} [n/(Sl)] \right\rangle. \tag{2.2}$$

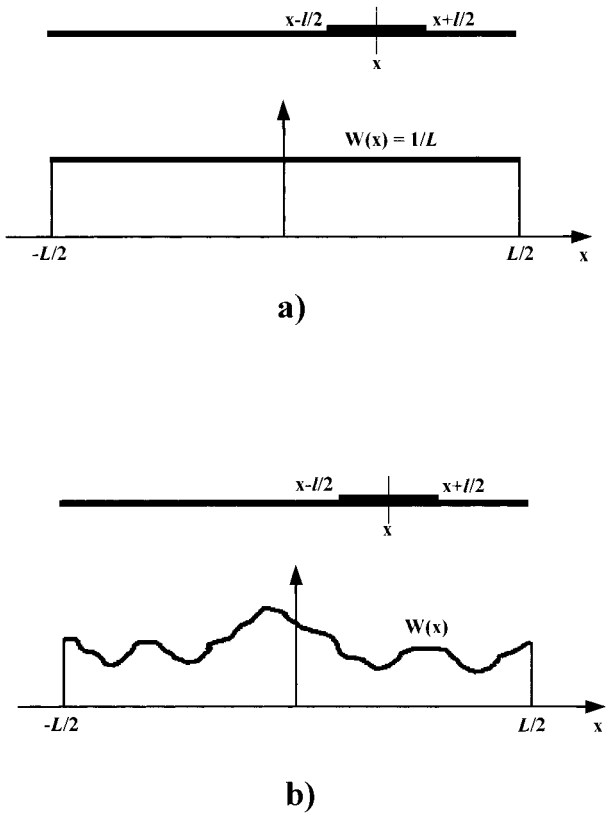

FIG. 1. Formation of Poisson distribution of the droplet count within a segment of length $[x - l/2, x + l/2]$: (a) formation of homogeneous Poisson distribution. Droplets fall within a cloud of length L extracted from a uniform distribution $W(x) = 1/L$. (b) The formation of nonstationary (inhomogeneous) Poisson distribution. Droplets fall within a cloud of length L extracted from a nonuniform finite distribution $W(x)$. The x axis is directed along the aircraft track in the cloud.

Hereinafter, the symbol $\langle\ \rangle$ denotes mathematical expectation. In this case the concentration is determined by the fraction of units in the series consisting of zeros and units.

We assume that the series of counts form the so-called Poisson flux (Feller 1966). When the droplet concentration along the aircraft track is constant, the series of counts forms a uniform Poisson flux. When droplet concentration along the aircraft track changes, the droplet flux becomes an inhomogeneous (generalized) Poisson process. Let us compare these two cases.

b. Poisson processes

1) THE UNIFORM POISSON DROP FLUX

Let us assume that a large number N of droplets extracted from a uniform distribution $W(x) = 1/L$ (λ = constant) fall within a cloud sample of length L, along the aircraft track (along the x axis; Fig. 1a). $W(x)$ is a distribution function of droplet coordinates along the aircraft track, so that the probability of a drop to fall into segment $(x, x + dx)$ is equal to $W(x)dx$. Here, W is proportional to the droplet concentration.

We assume that droplets fall within the cloud sample independently.

The probability of counts within a segment of length $l \ll L$ does not depend on the location of the segment along the track. The probability distribution of counts obeys the uniform Poisson distribution

$$P(n\,|\,\overline{n}) = \frac{\overline{n}^n}{n!}e^{-\overline{n}}, \tag{2.3}$$

where $\overline{n}$ is the parameter of the Poisson distribution. It represents the expected number of counts over a flight segment of length l, that is, $\overline{n} = \langle n\rangle$. Here, $\overline{n}$ does not depend on x and is related to λ as

$$\overline{n} = \langle n\rangle = S\int_{x-l/2}^{x+l/2} \lambda\, dx = Sl\lambda. \tag{2.4}$$

From the Poisson law the following relations for the second moments are also derived (Korn and Korn 1968):

$$\langle (n - \overline{n})^2\rangle = \overline{n}, \qquad \langle n^2\rangle = \overline{n}^2 + \overline{n}. \tag{2.5}$$

One can notice that the number of counts in disjoint segments is independent.

The Poisson law corresponds to the exponential distribution of intervals between counts along the aircraft track:

$$P(d\mid\lambda) = \lambda S\exp(-\lambda S d). \tag{2.6}$$

This approach is widely used when processing airborne droplet measurements and correcting droplet coincidence effects (see, e.g., the review by Brenguier et al. 1994).

2) THE INHOMOGENEOUS (GENERALIZED) POISSON DROP FLUX

As mentioned above, the droplet concentration in an actual cloud is not uniform. Let us consider a case where droplets extracted from a nonuniform finite distribution (Fig. 1b) fall within a cloud independently. It means that the probability of droplet location in different cloud regions is different, or in other words, that there exist droplet concentration inhomogeneities. Droplet concentration $\lambda(x)$ depends now on the position along the track. The expected number of counts $\langle n(x, l)\rangle$ over a segment of length l depends on the position and length of the segment. However, the probability of counts over l still follows the Poisson distribution (2.3), with parameter $\overline{n}(x, l)$ equal to $\langle n(x, l)\rangle$ (Feller 1966):

$$\overline{n}(x, l) = S\int_{x-l/2}^{x+l/2} \lambda(x)\, dx. \tag{2.7}$$

Similarly, (2.5) holds for the inhomogeneous Poisson process (Feller 1966):

$$\langle (n - \overline{n})^2 \rangle = \overline{n}(x, l) \quad \text{and}$$
$$\langle n^2 \rangle = \overline{n}^2(x, l) + \overline{n}(x, l). \tag{2.8}$$

In the following sections droplet concentration fluctuations will be described using the inhomogeneous Poisson distribution.

c. Characteristics of the cloud fine structure stipulated by drop inertia, as follows from theoretical considerations

In this section we determine the expected properties of the phenomena to be retrieved from drop arrival times series measured along cloud traverses.

There are several mechanisms forming drop concentration fluctuations in clouds. One of them is the inertia of droplets moving within a turbulent flow. According to the theory (e.g., Pinsky et al. 1999a), droplet inertia can lead to the formation of drop concentration fluctuations due to centrifugal forces resulting in deviation of droplet tracks from the surrounding air. The drop flux, therefore, turns out to be divergent in a nondivergent air flow. The divergence of the droplet flux responsible for the formation of drop concentration fluctuations is determined as (Maxey 1987)

$$\text{Div } V = -\frac{V_t}{g}\frac{\partial u_i}{\partial x_j}\frac{\partial u_j}{\partial x_i}, \tag{2.9}$$

where V_t is the terminal fall velocity of droplets in calm air, and u_i are the velocity components of a turbulent air flow.

Within the inertial range the kinetic energy turbulent spectrum obeys the $-5/3$ law: $E \sim k^{-5/3}$ (Monin and Yaglom 1975), where k is the wave number. Hence, the energetic spectrum of the turbulent velocity shear will be $E_{\text{shear}} \sim k^2 k^{-5/3} \sim k^{1/3}$. Thus, the spectrum of drop flux divergence defined by (2.9) $E_{\text{Div}} \sim k^{2/3}$. It means that formation of droplet concentration inhomogeneities due to the droplet inertia can be expected at the smallest spatial scales. However, at scales below about 1 cm, viscous effects become significant (e.g., Vohl et al. 1999) leading to a rapid decrease in all the spectra mentioned above. As a result, the maximum of the drop flux divergence turns out to be at scales of about one centimeter (Pinsky et al. 1999a; 2000). It is natural to assume that droplet concentration inhomogeneities caused by the droplet inertia will also take place at these centimeter scales. This conclusion is supported by direct numerical simulation of the motion of inertial particles within a turbulent flow (Wang and Maxey 1993).

Note that sharp jumps of droplet concentration at short distances of one to a few centimeters were found in situ observations in the vicinity of cloud boundaries (Pawlowska and Brenguier 1997). Such sharp transitions from droplet-free air to cloudy air can arise at the boundaries of air parcels entering a cloud. One can expect that the regions of these sharp jumps of droplet concentration cover only a small fraction of the whole cloud volume, in contrast to the fluctuations caused by drop inertia. We believe, therefore, that fluctuations of drop concentration caused by these boundary effects can hardly contribute significantly to the energy of centimeter-scale fluctuations obtained by averaging over the whole cloud traverse. This statement will be supported by a special test below.

The formation of droplet concentration inhomogeneities at larger scales can be caused by other mechanisms, for instance, by fluctuations of vertical velocity at the cloud base (Cooper 1989), entrainment of droplet-free air parcels with sizes from a few meters to several tens of meters at the cloud periphery (Grabowski and Clark 1991; Korolev and Mazin 1993), inhomogeneity of concentration of cloud condensation nuclei in the atmospheric boundary layer, and so on. These drop concentration fluctuations are related to turbulent fluctuations of velocity whose energy is known to increase with the size of turbulent vortices ($-5/3$ law). According to Warhaft (2000), passive scalar spectra at large Reynolds numbers typical of the atmosphere are close to $-5/3$ law (the inertial turbulent range). Thus, we can expect that the amplitude of related droplet concentration fluctuations increases with an increase of the spatial scale, being pronounced at scales of several meters to several tens of meters in accordance with the energetic spectra of turbulent velocities.

We expect, therefore, that centimeter-scale drop concentration fluctuations are well separated from fluctuations on larger scales.

d. Estimators for finescale drop concentration fluctuations

The variability of the number of counts during a measurement results from two contributions: random fluctuations due to the randomness of the counting process (Poisson process) and nonrandom fluctuations due to the variation of the droplet concentration along the aircraft trajectory.

The estimator should be able to reject efficiently the first contribution and keep only the information related to the variations of droplet concentration.

Estimators can be designed in different ways. Each estimator is based on some hypotheses selected to describe the statistical properties of a parameter to be estimated. Once these hypotheses have been identified, the estimation can be optimal in respect to these hypotheses.

An example of such an optimal estimator was presented by Pawlowska and Brenguier (1997). The estimator is a nonlinear optimal estimator, which is particularly suited for the detection of sharp transitions in the spatial evolution of droplet concentration. It provides the probability density function of droplet concentration along the flight track. The basic a priori hypothesis concerning droplet concentration is that this parameter is

driven by a random process, either a Poisson process, or a Brownian process. These hypotheses are suitable for the study of the interaction between turbulence and cloud microphysics, which allows the estimator to detect sharp uncorrelated transitions. However, an estimator of this type is inefficient when it is necessary to describe the statistical properties of a droplet field, such as the characteristic scale of concentration fluctuations.

The estimator developed here uses a different approach for the retrieval of such properties. It does not provide profiles of finescale droplet concentration, but it is suitable for the evaluation of the statistical properties of small-scale fluctuations of droplet concentration. In spite of the fact that the estimator proposed is not an optimal one (it is not based on any statistical criteria), it provides precise estimation of the characteristics of the centimeter-scale fine structure of droplet concentration.

3. Decomposition of droplet concentration

Droplet concentration varies along the cloud traverse. Airborne instruments regularly measure the profiles of cloud droplet concentration fluctuations with spatial scales less than of several meters to tens of meters. At the same time, we suppose that small-scale (centimeter scale) droplet concentration fluctuations are of substantially nonregular (noncoherent) nature, so that their profile along the aircraft track can hardly be calculated. Hence, we are going to estimate the profile of large-scale drop concentration variations along the cloud traverse, on the one hand, and some statistical parameters of small-scale variations, on the other hand.

As was mentioned in section 2d, each estimator is based on some assumptions selected to describe the statistical properties of a parameter to be estimated. Our assumptions based on the theoretical considerations of section 2c are there exist drop concentration fluctuations with scales of about one centimeter, caused by drop inertia. These fluctuations are well separated from large-scale fluctuations, caused by fluctuations of velocity, with some gap in the drop concentration fluctuations ranging from a few tens of centimeters to a few meters. Accordingly, we will represent droplet concentration in a cloud along the aircraft track as the sum of three terms:

$$\lambda(x) = \lambda_o + \lambda_1(x) + \lambda'(x), \tag{3.1}$$

where λ_o is the average droplet concentration over the cloud section; $\lambda_1(x)$ describes large-scale fluctuations of droplet concentration. Here, $\lambda'(x)$ is the small-scale noncoherent (nonregular) fraction of concentration fluctuations. We use the term ''coherent'' to identify large-scale concentration fluctuations with relatively slow changes of the phase along a cloud traverse. The terms ''noncoherent'' is used to identify small-scale concentration fluctuations with very fast and chaotic changes of the phase.

Decomposition (3.1) obeys well physical assumptions and allows us to give estimations of different components independently. This statement will be verified using corresponding tests (see section 6a).

Average droplet concentration over a cloud section of length L, λ_o can be determined as

$$\lambda_o = \frac{1}{L}\int_{-L/2}^{+L/2} \lambda(x)\, dx. \tag{3.2}$$

Coherent large-scale fluctuations of droplet concentrations $\lambda_1(x)$ can be represented by the Fourier series over the whole cloud length L as

$$\lambda_1(x) = \sum_{k=1}^{\infty} a_k \cos k\omega_o x + \sum_{k=1}^{\infty} b_k \sin k\omega_o x, \tag{3.3}$$

where $\omega_o = 2\pi/L$ is the main spatial harmonic (wave number) of expansion. The coefficients of Fourier series a_k and b_k are determined as:

$$a_k = \frac{2}{L}\int_{-L/2}^{L/2} \lambda_1(x) \cos k\omega_o x\, dx,$$

$$b_k = \frac{2}{L}\int_{-L/2}^{L/2} \lambda_1(x) \sin k\omega_o x\, dx. \tag{3.4}$$

Thus, the profile of large-scale fluctuations of droplet concentrations $\lambda_1(x)$ along the aircraft track is determined by the coefficients of the Fourier series a_k and b_k and the cloud length L.

In addition, large-scale droplet concentration fluctuations can be characterized by their total energy:

$$E_{\lambda_1} = \frac{1}{2}\sum_{k=1}^{\infty} (a_k^2 + b_k^2). \tag{3.5}$$

The square root of (3.5) is the mean square amplitude of large-scale fluctuations of droplet concentration.

The small-scale noncoherent fraction of concentration fluctuations $\lambda'(x)$ can be formally represented by the Fourier integral as

$$\lambda'(x) = \frac{1}{2\pi}\int_{-\infty}^{+\infty} Z^{\lambda'}(\omega) \exp(i\omega x)\, d\omega, \tag{3.6}$$

where $Z^{\lambda'}(\omega)$ is the amplitude spectrum, which is related to $\lambda'(x)$ by direct Fourier transform:

$$Z^{\lambda'}(\omega) = \int_{-L/2}^{+L/2} \lambda'(x) \exp(-i\omega x)\, dx. \tag{3.7}$$

The functions $\lambda'(x)$ and $Z^{\lambda'}(\omega)$ are extremely irregular (similar to random processes) and are unsuitable for the description of small-scale concentration fluctuations. It is clear that centimeter-scale concentration fluctuations are highly incoherent because of the nature of a turbulent flow. The values of small-scale droplet concentration fluctuations must be independent at scales greater than the spatial correlation scale, which according to Pinsky et al. (1999a) is about a few centimeters. Taking into

account that the cloud length is about several hundred meters, the phase of centimeter-scale fluctuations changes over this distance many times. Lack of correlation between phases of small-scale droplet fluctuations of close frequencies hinders the utilization of the Fourier integral (3.6) for the description of small-scale concentration fluctuations.

Therefore, the fluctuations will be characterized by their energetic parameters (without allowing for phase characteristics): by the energy spectrum $F^{\lambda'}(\omega)$ and correlation function $B^{\lambda'}(l)$ obtained by averaging over the whole cloud length L. The energy spectrum $F^{\lambda'}(\omega)$ and correlation function $B^{\lambda'}(l)$ can be defined as

$$F^{\lambda'}(\omega) = \frac{2}{L}|Z^{\lambda'}(\omega)|^2 \quad \text{and} \tag{3.8}$$

$$B^{\lambda'}(l) = \frac{1}{L}\int_{-L/2}^{+L/2} \lambda'\left(x - \frac{l}{2}\right)\lambda'\left(x + \frac{l}{2}\right) dx. \tag{3.9}$$

The energy spectrum and the corresponding correlation function are related through the following pair of Fourier transforms:

$$F^{\lambda'}(\omega) = 2\int_{-L/2}^{+L/2} B^{\lambda'}(l)\,\exp(-i\omega l)\,dl \tag{3.10}$$

$$B^{\lambda'}(l) = \frac{1}{4\pi}\int_{-\infty}^{+\infty} F^{\lambda'}(\omega)\,\exp(i\omega l)\,d\omega. \tag{3.11}$$

The energy spectrum $F^{\lambda'}(\omega)$ characterizes the distribution of concentration fluctuations with respect to the spatial wave number or the characteristic scale. The energy of small-scale noncoherent concentration fluctuations can be calculated as

$$E_{\lambda'} = B^{\lambda'}(0) = \int_{-\infty}^{+\infty} F^{\lambda'}(\omega)\,d\omega. \tag{3.12}$$

Thus, droplet concentration in clouds is divided into three components. Each component can be characterized by its contribution to the total ''energy'' of droplet concentration variation. Comparison of these energy components $E_{\lambda'}$ and E_{λ_1} with λ_o^2 allows us to estimate the relative strength of the corresponding droplet concentration fluctuations and the mechanisms causing the fluctuations.

Some comments to the decomposition (3.1) are required. We use the terminology ''regular'' versus ''nonregular'' or ''coherent'' versus ''noncoherent'' to stress the difference between fluctuations, profile of which can be restore from measurements and those, which profile cannot be reproduced (calculated), respectively. The state-of-the-art Fast FSSP allows one to restore profiles of drop concentration fluctuations beginning with scales less than of several meters. We believe, however, that the errors in concentration profile restoring are significant on scales less than 1 m increasing with a decrease in scale, so that it is actually impossible to restore the profile of concentration fluctuations at scales below about 10 cm.

The first type of the fluctuations we calculate using the Fourier series, that is, as a sum of products of deterministic functions and unknown a priori (random) coefficients. Decomposition of the droplet concentration (3.1) is valid for a statistical analysis of any series containing coherent and noncoherent components, independently of the physical nature of these fluctuations. As a matter of fact, total drop concentration $\lambda(x)$ could be represented using the Fourier integral. In this case decomposition (3.1) would mean a simple separation of the whole range of wavenumbers into two subranges with wavenumbers larger and smaller than a certain value chosen. Drop concentration fluctuations relating to each subrange can be analyzed by different methods. The only requirement to be obeyed is that the subranges should not overlap.

It means that the number of harmonics in the Fourier series (3.3) representing large-scale fluctuations, should be, on the one hand, large enough to describe adequately the large-scale profile of droplet concentration along the traverse, and, on the other hand, it should be less than the number of harmonics corresponding to the spatial scale of several centimeters. In the calculations (see section 6) series (3.3) was truncated at a certain maximum value of k, corresponding to the spatial scale of about 4 m. Analysis of the case study shows that the amplitude of the harmonics decreases with an increase of their number. This result agrees with our assumption that the amplitude of large-scale fluctuations increases with the wavelength. At wavelengths shorter than 4 m, phases of harmonics become nonregular, so that these harmonics play the role of noise along with natural Poisson fluctuations. Thus, an increase in the number of harmonics above a certain value does not improve the representation of large-scale droplet concentration fluctuations.

4. Relationship between the components of drop concentration fluctuations and cloud average parameters

a. Representation of the Poisson distribution parameter $\overline{n}(x, l)$ within segment $[x - l/2, x + l/2]$

Using (3.1), the Poisson distribution parameter $\overline{n}(x, l)$ within segment $[x - l/2, x + l/2]$ can be represented as the sum of mean, coherent and small-scale noncoherent fluctuations:

$$\overline{n}(x, l) = \overline{n_o}(l) + \overline{n_1}(x, l) + \overline{n'}(x, l). \tag{4.1}$$

The components in (4.1) can be obtained by substituting (3.2), (3.3) and (3.6) into (2.7). One can show that the components are as follows (see appendix A):

$$\overline{n_o}(l) = \lambda_o Sl;$$

$$\overline{n_1}(x, l) = \sum_{k=1}^{\infty} A_k(l) \cos k\omega_o x + \sum_{k=1}^{\infty} B_k(l) \sin k\omega_o x$$

$$\overline{n'}(x, l) = \frac{S}{\pi} \int_{-\infty}^{+\infty} Z^{\lambda'}(\omega) \exp(i\omega x) \sin\frac{\omega l}{2} \frac{d\omega}{\omega}. \quad (4.2)$$

The Fourier coefficients in (4.2) are related to the Fourier coefficients (3.4) as

$$A_k(l) = \frac{2Sa_k}{k\omega_o} \sin\frac{k\omega_o l}{2} \qquad B_k(l) = \frac{2Sb_k}{k\omega_o} \sin\frac{k\omega_o l}{2}. \quad (4.3)$$

When $k\omega_o l/2$ is small (say, less than 0.1), Eq. (4.3) can be simplified as

$$A_k(l) = a_k Sl; \qquad B_k(l) = b_k Sl. \quad (4.3')$$

We will also utilize the square of the Poisson distribution parameter in the segment of length l:

$$\overline{n}^2(x, l) = [\overline{n_o}(l) + \overline{n_1}(x, l) + \overline{n'}(x, l)]^2. \quad (4.4)$$

Expressions (4.1), (4.2), and (4.4) will be used to determine cloud-averaged values, which depend on the segment length l only.

b. Poisson parameter averaged over the whole cloud section L

The values averaged over the whole cloud length will be denoted by the symbol "˜."

The Poisson distribution parameter averaged over the length L of cloud, $\tilde{\overline{n}}(l)$ is determined as

$$\tilde{\overline{n}}(l) = \frac{1}{L} \int_{-L/2}^{+L/2} \overline{n}(x, l)\, dx. \quad (4.5)$$

Substitution of (4.1) and (4.2) into (4.5) yields (see appendix B)

$$\tilde{\overline{n}}(l) = \lambda_o Sl + \frac{S}{2\pi L} \int_{-\infty}^{+\infty} Z^{\lambda'}(\omega) \sin\frac{\omega L}{2} \sin\frac{\omega l}{2} \frac{d\omega}{\omega^2}$$

$$\approx \lambda_o Sl + \frac{Sl}{L} Z^{\lambda'}(0). \quad (4.6)$$

As can be seen from (3.7), the term $(Sl/L)Z^{\lambda'}(0)$ is equal to zero (because cloud averaged values of concentration fluctuations λ' are equal to zero). As a result, we have

$$\tilde{\overline{n}}(l) = \lambda_o Sl. \quad (4.7)$$

From (4.7) we can conclude that the cloud averaged Poisson distribution parameter $\tilde{\overline{n}}(l)$ contains information about the averaged droplet concentration λ_o only. It can be calculated as the ratio $\tilde{\overline{n}}(l)/(Sl)$. This ratio does not depend on the segment length l.

c. Additional cloud section averaged values

We also introduce additional cloud averaged values $\tilde{n}_{A_k}(l)$ and $\tilde{n}_{B_k}(l)$, which characterize large-scale coherent droplet concentration variations $\lambda_1(x)$. These values are determined as follows:

$$\tilde{n}_{A_k}(l) = \frac{2}{L} \int_{-L/2}^{+L/2} \overline{n}(x, l) \cos(k\omega_o x)\, dx, \quad \text{and} \quad (4.8)$$

$$\tilde{n}_{B_k}(l) = \frac{2}{L} \int_{-L/2}^{+L/2} \overline{n}(x, l) \sin(k\omega_o x)\, dx, \quad (4.8')$$

where $\omega_o = 2\pi/L$ is the main spatial harmonic of expansion.

Using (4.1), (4.2), and (4.3′), we can see that (see appendix B)

$$\tilde{n}_{A_k}(l) = A_k(l) \approx a_k Sl, \quad \tilde{n}_{B_k}(l) = B_k(l) \approx b_k Sl. \quad (4.9)$$

One can see that (4.9) connects values $\tilde{n}_{A_k}(l)$ and $\tilde{n}_{B_k}(l)$ with the Fourier coefficients a_k and b_k in (3.3), which, in its turn, permit us to calculate the coherent large-scale part of droplet concentration variations.

d. The cloud section–averaged square of the Poisson distribution parameter

Expressions (4.7) and (4.9) permit us to calculate the first two components of droplet concentration in (3.1). Now the problem is to evaluate the noncoherent part of droplet concentration fluctuations. To do this, let us calculate the cloud-averaged square of the Poisson distribution parameter within the segment l as:

$$\widetilde{\overline{n}^2}(l) = \frac{1}{L} \int_{-L/2}^{L/2} \overline{n}^2(x, l)\, dx$$

$$= \widetilde{\overline{n}_o^2}(l) + \widetilde{\overline{n}_1^2}(l) + \widetilde{\overline{n}'^2}(l). \quad (4.10)$$

When deriving (4.10), the fact that the integrals of products of different terms in (4.4) are equal to zero was taken into account. This fact results from mutual noncoherence of the terms, as well as from the orthogonality of the functions $\sin(k\omega_o x)$ and $\cos(j\omega_o x)$.

Using (4.2) (see Appendix B), we get

$$\widetilde{\overline{n}_o^2}(l) = (\lambda_o Sl)^2 \quad (4.11)$$

$$\widetilde{\overline{n}_1^2}(l) = \frac{1}{2} \sum_{k=1}^{\infty} (A_k^2 + B_k^2)$$

$$= 2S^2 \sum_{k=1}^{\infty} \frac{a_k^2 + b_k^2}{\omega_o^2 k^2} \sin^2\left(\frac{k\omega_o l}{2}\right)$$

$$\approx \frac{(Sl)^2}{2} \sum_{k=1}^{\infty} (a_k^2 + b_k^2) \quad (4.12)$$

$$\widetilde{\overline{n}'^2}(l) = \frac{S^2}{\pi} \int_{-\infty}^{\infty} F^{\lambda'}(\omega) \sin^2\left(\frac{\omega l}{2}\right) \frac{d\omega}{\omega^2}. \quad (4.13)$$

Thus, the function $\widetilde{\overline{n}^2}(l)$ contains information about all three components of the droplet concentration $\lambda(x)$ in (3.1). The second derivative of (4.10) with respect to l can be written as follows (see appendix B):

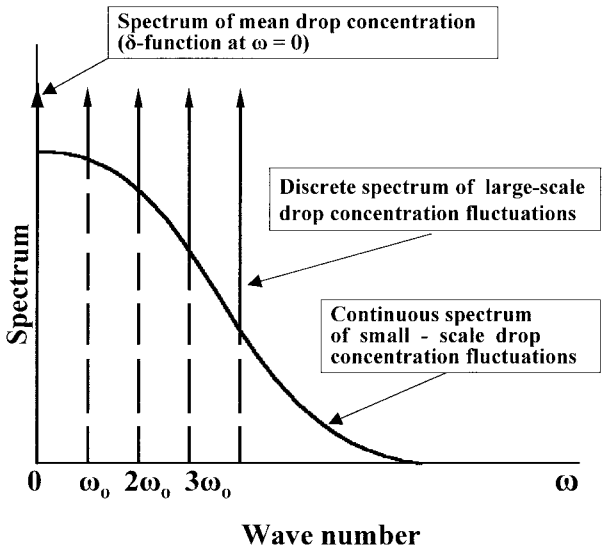

FIG. 2. Sketch of the energy spectrum of droplet concentration.

$$\frac{1}{2S^2}\frac{d^2\widetilde{\overline{n}^2}}{dl^2} = \lambda_o^2 + \frac{1}{2}\sum_{k=1}^{\infty}(a_k^2 + b_k^2)\cos(k\omega_o l) + B^{\lambda'}(l). \quad (4.14)$$

The physical meaning of (4.14) is the following: its right side is the covariation function of total fluctuations of droplet concentration. For example, when $l = 0$ it consists of three terms: powers of mean, large-scale coherent, and small-scale noncoherent components of the concentration. All three components are noncorrelated with respect to each other. Because of this fact, the total power is the sum of powers of the components.

According to (4.14), the energy spectrum of droplet concentration [Fourier transform of the right side of (4.14)] consists of three parts: the spectrum of the constant component (delta function at zero frequency), the discrete spectrum of a large-scale component (delta functions at spatial frequencies ω_o, $2\omega_o$, . . .), and the continuous energy spectrum of the small-scale component of droplet concentration fluctuations. A sketch of the spectrum is presented in Fig. 2.

Expressions (4.7), (4.9), and (4.14) permit us to obtain full information about drop concentration fluctuations in a cloud.

5. Statistical estimations and evaluations of errors

In the previous sections theoretical relationships for the parameters of an inhomogeneous Poisson distribution with different components of droplet concentration were obtained.

These relationships allow us to propose the following estimations of droplet concentration components by analysis of the observed data. The estimated values will be denoted with $\hat{}$.

Let $n(x, l)$ be an in situ measured number of droplets located within any segment $[x - l/2, x + l/2]$. This random value is distributed according to the generalized Poisson distribution (2.3). So, when the segment length l is equal to the distance passed by the aircraft between subsequent pulses of the FFSP (1/16 μs), the number of droplets in these segments of minimum length can be either one or zero.

Cloud-averaged droplet concentration is calculated by averaging the number of droplets in segments of length l over the whole cloud length L. Using similarities with (4.5) and (4.7), cloud-averaged droplet concentration can be estimated as

$$\hat{\lambda}_o = \frac{1}{Sl}\frac{1}{L-l}\int_{-(L-l)/2}^{(L-l)/2} n(x, l)\,dx. \quad (5.1)$$

For the calculation of the Fourier coefficients required to determine coherent large-scale concentration fluctuations we can use the following estimations (see similar expressions 4.8 and 4.9):

$$\hat{a}_k = \frac{1}{Sl}\frac{2}{L-l}\int_{-(L-l)/2}^{(L-l)/2} n(x, l)\cos(k\omega_o x)\,dx \quad (5.2)$$

$$\hat{b}_k = \frac{1}{Sl}\frac{2}{L-l}\int_{-(L-l)/2}^{(L-l)/2} n(x, l)\sin(k\omega_o x)\,dx. \quad (5.2')$$

Estimations (5.1)–(5.2) permit us to evaluate the profile of the large-scale component of droplet concentration fluctuations along the aircraft track as

$$\hat{\lambda}(x) = \hat{\lambda}_o + \sum_{k=1}^{k_{\max}}\hat{a}_k\cos(k\omega_o x) + \sum_{k=1}^{k_{\max}}\hat{b}_k\sin(k\omega_o x), \quad (5.3)$$

where $\omega_o = 2\pi/L$.

The estimation of the mean square of drop concentration as a function of the segment length is taken in the form

$$\widehat{\widetilde{\overline{n}^2}}(l) = \frac{1}{L-l}\int_{-(L-l)/2}^{(L-l)/2} n^2(x, l)\,dx. \quad (5.4)$$

The correlation function of small-scale fluctuations can be estimated by double differentiation of (5.4) (see 4.14)

$$\hat{B}^{\lambda'}(l) = \frac{1}{2S^2}\frac{d^2\widehat{\widetilde{\overline{n}^2}}}{dl^2} - \hat{\lambda}_o^2 - \frac{1}{2}\sum_{k=1}^{k_{\max}}(\hat{a}_k^2 + \hat{b}_k^2). \quad (5.5)$$

The Fourier transform of the estimated correlation function yields the estimation of the energy spectrum of small-scale concentration fluctuations $\hat{F}^{\lambda'}$.

Derivatives in (5.5) were calculated numerically using the formula (Korn and Korn 1968): $y'_k = (1/10\Delta x)(-2y_{k-2} - y_{k-1} + y_{k+1} + 2y_{k+2})$. Here $\Delta x = 6.25 \times 10^{-4}$ cm was determined by the time resolution of the FFSSP. Actually, the derivative has been calculated with respect to time and then recalculated into the derivative with respect to x, taking into account the aircraft speed (about 100 m s^{-1}).

The estimation cannot be regarded as optimal one in

the statistical sense because it has not been obtained using certain statistical criteria. Nevertheless, the estimation has some advantages:

- It has no bias or else the bias is negligible (see appendix C).
- Calculations of the estimated values have been carried out within the whole swept volume along the aircraft track in a cloud. This volume contains a great number of droplets. It allows us to suggest that averaging errors are small. The high precision of the estimations has been proven using special tests (see next section).
- The estimations are obtained using comparably simple formulas providing an effective computational algorithm required to process a large volume of observed data.

There is, however, a limitation to such a global approach. The parameters derived using a statistical technique characterize the whole sample, and it is implicitly assumed that the statistical properties of the droplet field are uniform over the sample. When this is not the case, the procedure must be repeated over those specific subsamples to characterize their properties. An example of the procedure will be presented in section 7.

Note that possible instrumental errors in droplet counting by the Fast FSSP are discussed in detail by Brenguier et al. (1998). The errors turned out to be negligible even in case of droplet concentration as high as 2000 cm^{-3}.

6. Tests of the algorithm

a. Test description

To verify the validity of the algorithm developed in previous sections, special tests have been conducted. The tests pursued the following aims:

- verification of the ability of the algorithm to reveal the existence of centimeter-scale droplet concentration fluctuations, and evaluation of the accuracy of estimation of their amplitude; and
- verification of the ability of the algorithm to retrieve large-scale drop concentration fluctuations and evaluation of the accuracy of the estimation.

The profile of droplet concentration $\lambda(x)$ consisted of three parts in accordance with (3.1): $\lambda(x) = \lambda_o + \lambda_1(x) + \lambda'(x)$. In all tests the mean drop concentration λ_o was set equal to 200 cm^{-3}.

To investigate the effects of large-scale droplet fluctuations on the estimations of small-scale fluctuations, three types of $\lambda_1(x)$ were used: (i) no large-scale fluctuations have been assumed [$\lambda_1(x) = 0$]; (ii) $\lambda_1(x)$ is represented by a rectangle impulse of drop concentration, simulating effects of sharp changes of droplet concentration at the cloud periphery; and (iii) ''real'' large-scale fluctuations were represented by 76 harmonics of the Fourier series expansion, obtained over a 300-m length section of a simulated cloud. This corresponds to a minimum wavelength of 4 m. The last case aims at revealing the possible impact of a more realistic large-scale profile of drop concentration fluctuations on the estimation of centimeter-scale droplet concentration fluctuations.

We have used two different approaches to simulate small-scale droplet concentration fluctuations $\lambda'(x)$.

1) AUTO REGRESSION (AR)

The autoregression random process of the first order (Yaglom 1987) expressed as

$$\lambda'_{t+1} = a\lambda'_t + \sigma\varepsilon_{t+1}, \ (a < 1), \tag{6.1}$$

where ε_t is a sequence of independent normally distributed random values with a zero mean value and a unit dispersion. The process, determined by the recursive expression (6.1), is a normal random sequence with a zero mean value and the dispersion given as (Yaglom 1987)

$$\sigma^2_{\lambda'} = \frac{\sigma^2}{1 - a^2}. \tag{6.2}$$

The correlation function of this random sequence is exponential:

$$R(\tau) = \sigma^2_{\lambda'} \exp(-\gamma\tau), \tag{6.3}$$

where $\gamma = -\ln a$, $a < 1$.

Various values of the parameters of small-scale droplet concentration fluctuations were simulated by setting the values of the parameters $\sigma^2_{\lambda'}$ and a.

2) TELEGRAPH SIGNAL (TS)

In this test, small-scale concentration fluctuations are simulated by a random telegraph signal. This signal represents a sequence of random positive and negative jumps of concentration with a given amplitude $\sigma_{\lambda'}$. The events that during a subsequent time step Δt (determined by the operative 16-MHz pulse repetition frequency) a jump will occur are independent and take place with a probability determined as

$$P = \frac{1}{2}[1 - \exp(-\gamma\Delta t)]. \tag{6.4}$$

The telegraph signal has the same exponential correlation function (6.3) as the process of autoregression. In both tests, parameter γ characterizes a typical timescale of droplet concentration fluctuations measured during an aircraft flight. When the aircraft velocity is known this timescale can be easily transformed into a characteristic length scale.

The main difference between the tests is that the process of autoregression simulates smoothed droplet concentration fluctuations, while the telegraph signal simulates sharp jumps of the concentration.

TABLE 1. Parameters and results of test experiments.*

No. test			1	2	3	4	5	6
Type of signal			—	AR	AR	AR	TS	TS
$\sigma_{\lambda'}$ (cm^{-3}) (test value)			0	20	40	40	40	40
Estimation $\hat{\sigma}_{\lambda'}$ (cm^{-3})	Type of large-scale drop concentration fluctuations	No	5.8	20.99	43.52	46.75	40.71	43.24
		Rectangular	5.8	22.04	40.05	45.24	41.22	43.56
		Realistic	3.2	20.09	40.08	51.2	46.4	41.6
$\sigma_{\lambda'}/\lambda_o$ (%) (test value)			0	10	20	20	20	20
Estimation $\hat{\sigma}_{\lambda'}/\lambda_o$ (%)	Type of large-scale drop concentration fluctuations	No	2.91	10.5	20.73	23.38	20.36	21.62
		Rectangular	2.91	11.02	20.03	22.62	20.62	21.78
		Realistic	1.6	10.5	20.4	25.6	23.2	20.8
l_{cor} (test)			—	1.0	1.0	0.2	0.5	1.0
Estimation $\hat{l}_{cor}$ (cm)	Type of large-scale drop concentration fluctuations	No	0.2	1.22	0.98	0.28	0.58	0.93
		Rectangular	0.2	1.04	1.11	0.29	0.58	0.90
		Realistic	0.3	0.8	1.0	0.3	0.49	0.99

* Notations: AR: Autoregression random process. TS: Random telegraph signal. Here λ_o is the mean drop concentration; $\sigma_{\lambda'}$ (cm^{-3}) is the rms amplitude of small-scale drop concentration fluctuations; l_{cor} (cm) is the correlation length, at which the correlation function decreases 2.7 times. Two types of large-scale drop concentration fluctuation profiles are used: rectangular and realistic.

The list of tests conducted, as well as the conditions and results of the tests, are presented in Table 1. The following parameters of small-scale droplet concentration fluctuations were chosen: To verify the ability of the approach to retrieve the amplitude of small scale droplet concentration fluctuations, the values of $\sigma_{\lambda'}$ were set to 20 and 40 cm^{-3}, which correspond to 10% and 20% of the mean droplet concentration. To verify the validity of the method, a case with no centimeter-scale concentration fluctuations ($\sigma_{\lambda'} = 0$) has also been simulated.

To verify the ability of the approach to retrieve the characteristic spatial scales of small-scale droplet concentration fluctuations, the correlation length l_{cor} was set to 0.2, 0.5, and 1 cm as indicated in Table 1. Taking into account that the operative pulse repetition frequency of the FFSSP is 16 MHz and that the aircraft velocity is equal to 100 m s^{-1}, these correlation lengths correspond to γ^{-1} values of 320, 800, and 1600, respectively.

Utilizing the generated sequence of droplet concentration, a series of droplet arrival times was simulated using the technical characteristics of the FFSSP mentioned above. The effective cross section of the FFSSP laser beam was set equal to 3.25 mm^2.

The random series of droplet arrival times were generated using the current values of droplet concentration simulated by either (6.1) or (6.4). For this purpose a generator of exponentially distributed independent random values was used. According to (2.6), the current value of droplet concentration determines the parameter of the distribution.

The basic generator of uniformly distributed random values described by Abramovitz and Stegan (1964) was used both for the simulation of droplet concentration and droplet interarrival times. It has a large repeating period of 2^{47}, which permitted us to form large model series of droplet arrival times.

As a result, series of droplet arrival times were generated in a form similar to that obtained by in situ FFSSP measurements. These files were treated using the algorithm described by (5.1)–(5.5).

b. Results of the tests

The results of tests are summarized in Table 1 and illustrated in Figs. 3–6. In Figs. 3a,b the profiles of large-scale droplet concentration variations along the aircraft track, $\lambda_o + \lambda_1(x)$, are plotted for six tests (Table 1). One can see that the algorithm retrieves well large-scale droplet concentration variations, irrespective of the values of the parameters of small-scale droplet concentration fluctuations.

Figure 4 shows (as an example) the correlation function of small-scale droplet concentration fluctuations $\hat{B}^{\lambda'}(l)$ as a function of the distance between two points in a cloud along the aircraft track (along the x axis) for droplet concentration fluctuations with root-mean-square amplitudes of 20% of the mean concentration (test 3 in Table 1) for the case of ''realistic'' large-scale droplet concentration fluctuations. High-frequency variations of the correlation function caused by the noise induced by natural (uniform) Poisson fluctuations of droplet counts were eliminated in the Fig. 4 by fitting the correlation functions with an exponential function (least-root-mean-square algorithm). The correlation function deduced as a result of the fitting is plotted as a solid line. One can see that such fitting effectively eliminates high-frequency fluctuations making it pos-

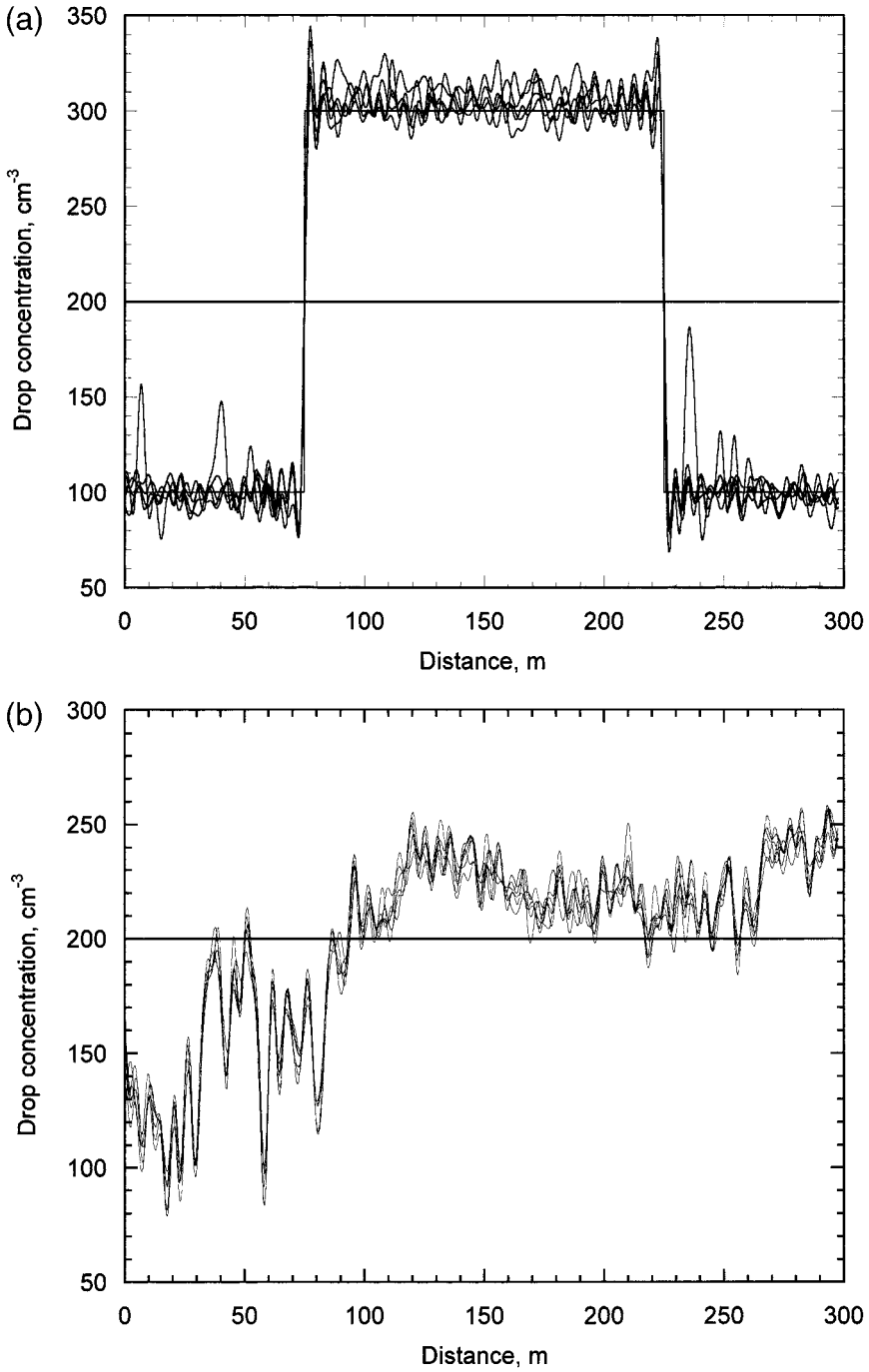

FIG. 3. Model profiles of large-scale droplet concentration $\lambda_o + \lambda_1(x)$ along x in all test calculations (see Table 1): (a) rectangular large-scale profile and (b) realistic large-scale profile constructed using 76 Fourier harmonics. One can see efficient retrieval of large-scale droplet concentration variations independent on the parameters of small-scale concentration fluctuations.

sible to evaluate the amplitude and correlation length of the signal. We have used such fitting for the evaluation of amplitudes and correlation lengths in all the tests presented in Table 1.

Figure 5 shows the correlation functions of small-scale droplet concentration fluctuations $\hat{B}^{\lambda'}(l)$ (to be more exact, exponential approximations of the correlation functions) as a function of the distance between two points in a cloud along the aircraft track (along the x axis) for droplet concentration fluctuations with root-mean-square amplitudes of 0%, 10% and 20% of the mean concentration (tests 1–3 in Table 1) for all types

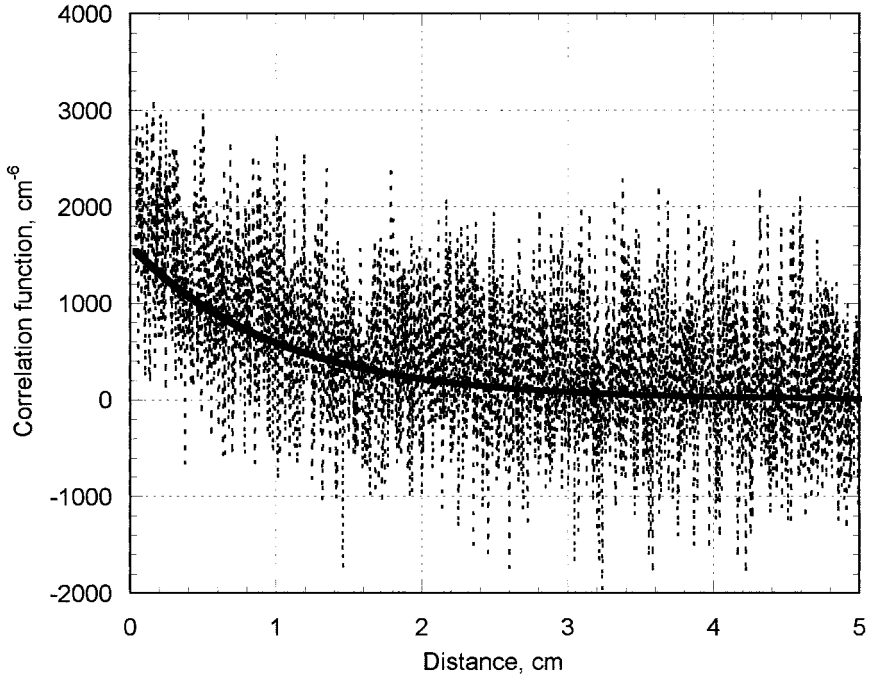

FIG. 4. The correlation function of small-scale droplet concentration fluctuations $\hat{B}^{\lambda'}(l)$ as a function of the distance between two points in a cloud along the aircraft track (along the x axis) for droplet concentration fluctuations with rms amplitudes of 20% of the mean concentration (test 3 in Table 1) for the case of the realistic large-scale droplet concentration fluctuations.

of large-scale droplet concentration fluctuations. Small-scale fluctuations in these tests have the same correlation lengths (1 cm) and different amplitudes (0%, 20%, and 40% of the mean value of drop concentration). Theoretical correlation functions are also presented in the figure to facilitate comparison (solid lines). The value of the correlation function at $l = 0$ is the power of small-scale droplet concentration fluctuations. In test 1 (Table 1) in which no small-scale fluctuations were introduced, the correlation function indicates no pronounced maximum at $l = 0$. According to Table 1, the mean error in revealing of the amplitude of small-scale concentration fluctuations is 5% and does not exceed 25% in all tests.

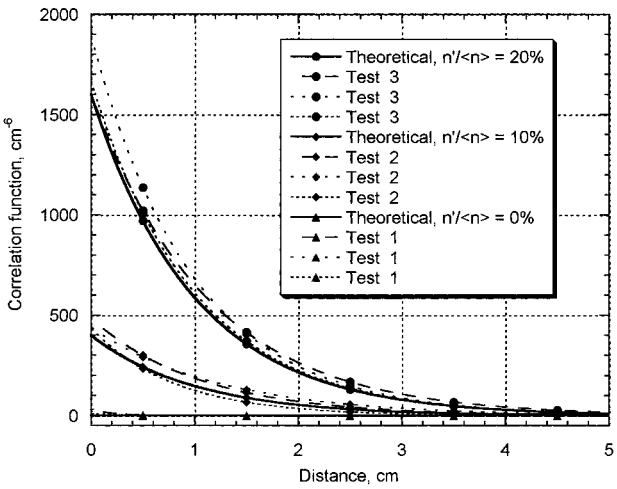

FIG. 5. Exponential approximations of the estimated correlation functions for small-scale droplet concentration fluctuations with rms amplitudes of 0%, 10%, and 20% of the mean droplet concentration (tests 1 to 3 in Table 1) for all types of large-scale droplet concentration fluctuations. Small-scale fluctuations have the same correlation lengths (1 cm) and different amplitudes (0%, 20%, and 40% of the mean value of drop concentration). Theoretical correlation functions are presented for sake of comparison (solid lines).

Figure 6 illustrates the sensitivity of the method to changes of the correlation length scale. The figure shows estimated correlation functions $\hat{B}^{\lambda'}(l)$ (exponential approximations of the correlation functions) for cases when the correlation length scale was set to 0.2, 0.5, and 1 cm (tests AR3, AR4, and TS5 in Table 1, respectively) for all types of large-scale droplet concentration fluctuations presented in the table. Theoretical correlation functions are also presented in the figure for the sake of comparison (solid lines). In all these tests the root-mean-square values of drop concentration inhomogeneity amounted to 20% of the mean value of drop concentration.

The estimated value of the correlation length was determined as the length at which the amplitude of the correlation function decreases by a factor of 2.7. We can see that the retrieved values are very close to those preset initially (1 cm). According to Table 1, the mean error in revealing of the correlation length is about 10% and does not exceed 30%.

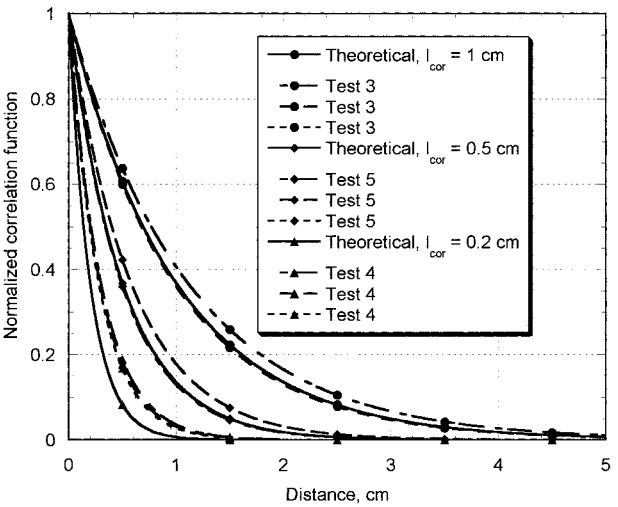

FIG. 6. Exponential approximations of the estimated correlation functions for cases in which the correlation length scale was set to 0.2, 0.5, and 1 cm (tests 3–5 in Table 1, respectively) for all types of large-scale droplet concentration fluctuations presented in the table. Theoretical correlation functions are also presented for sake of comparison (solid lines). In these tests the rms values of drop concentration inhomogeneity amounted to 20% of the mean value of drop concentration.

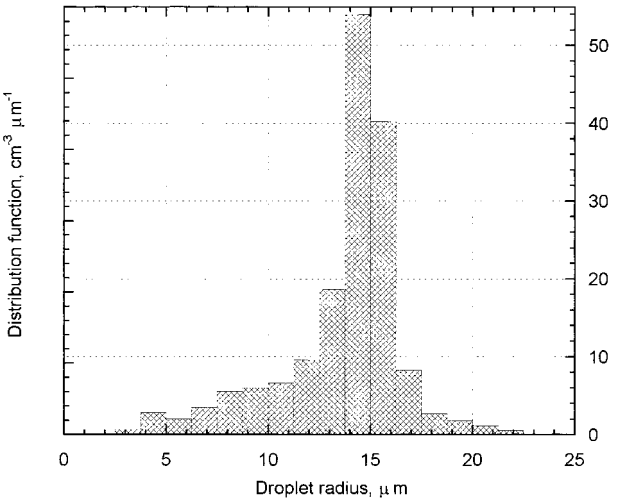

FIG. 7. The droplet size distribution in a cumulus cloud analyzed in the case study.

We can see that the results of TS tests compare well with those of AR tests. In both cases the estimated values are close to those preset. Estimation error increases as the correlation length decreases. We attribute this result to the fact that the correlation length tends to the mean distance between droplets (0.17 cm in our case) and the noise caused by the natural (homogeneous) Poisson process hinders the retrieval of small-scale concentration fluctuations. Besides, at a spatial distance typical of scales of droplet concentration fluctuations several droplets must be located (on the average), otherwise, the concept of droplet concentration fluctuations does not make sense.

The analysis of the results of testing can be summarized as follows.

(i) The method proposed is efficient as regards reproducing the amplitude and the correlation length of small-scale droplet concentration fluctuations.

(ii) The type of the profile of large-scale concentration fluctuations does not influence parameters of centimeter-scale drop concentration fluctuations. The parameters of centimeter-scale drop concentration fluctuations are retrieved equally well in case of no large-scale fluctuations assumed, rectangle and realistic profiles of large-scale drop concentration fluctuations. Despite the fact that the rectangle profile being expanded into the Fourier series contains centimeter-scale harmonics, their energy is negligibly small as compared with that of expected centimeter-scale concentration fluctuations existing over the whole cloud traverse. It means that small- and large-scale fluctuations are well separated even in case of very erratic large-scale drop concentration profiles.

(iii) The algorithm retrieves the profiles of large-scale concentration variations with a high accuracy.

7. Results of in situ data processing

Below are presented the results of the analysis of a droplet concentration structure using a sample of FFSSP data measured by an aircraft in a cumulus cloud with a length of $L = 350$ m at the flight level of 2.17 km. The speed of aircraft was about 100 m s^{-1}. The total sensitive section of the FFSSP (perpendicular to the aircraft track) used for droplet counting was 3.25 mm^2.

The mean droplet size distribution over the cloud section is presented in Fig. 7. The spectrum is typical of cumulus clouds. One can see that the spectrum is centered at a droplet radius of about 14 μm. Thus, in the cumulus cloud analyzed droplets are comparably large and have a significant inertia. According to the theory (Pinsky et al. 1999a), we can expect significant small-scale concentration fluctuations in this case.

The results of the calculations can be summarized as follows.

Large-scale coherent components of droplet concentration fluctuations were calculated using the evaluations of the Fourier coefficients (5.2) and (5.2′). When calculating the coefficients, the segment length was set equal to 6.25×10^{-4} cm, which corresponds to the pulse repetition frequency of 16 MHz used in the FFSSP. In this case the number of droplets in any segment is equal to 1 or to 0.

Additional calculations of harmonic power as a function of harmonic number were conducted. The results (not shown) indicate that the amplitude of the harmonics with a number greater than about 70 (in the particular case study) actually lies within the noise level. So, the

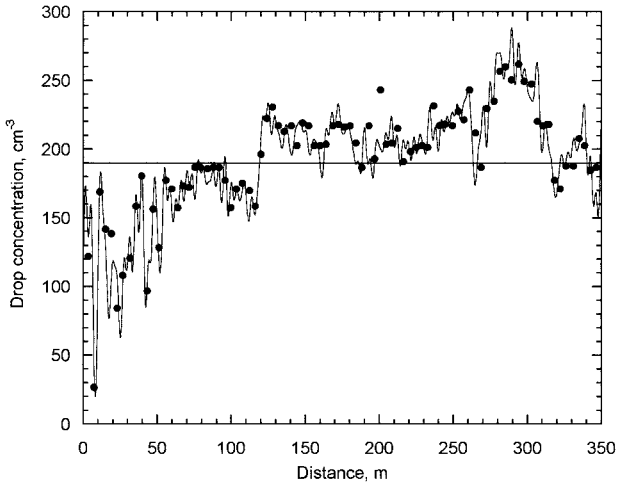

FIG. 8. The sum of the mean value and the coherent component of drop concentration $\lambda_o + \lambda_1(x)$ along the whole cloud traverse. The droplet concentration obtained from FFSSP measurements using the optimal estimator by Pawlowska and Brenguier (1997) is presented for comparison (denoted by thin line with points).

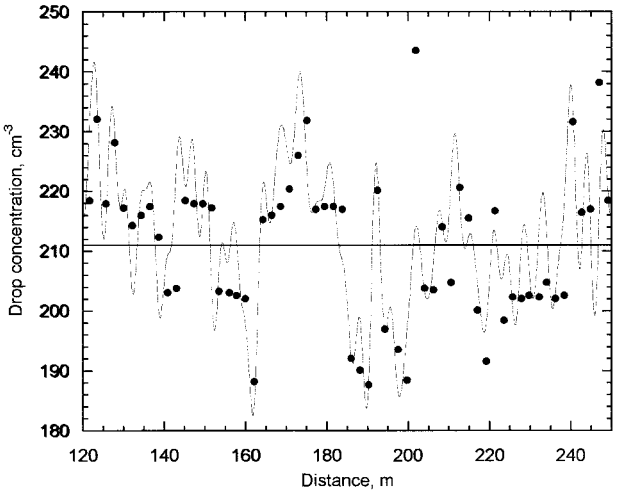

FIG. 9. The same as in Fig. 8, but for the adiabatic cloud core.

first 76 terms (harmonics) of the Fourier series (k ranging from 1 to 76) were used. These harmonics cover spatial scales from 350 down to 4.6 m.

The sum of the mean value and the coherent component of droplet concentration $\lambda_o + \lambda_1(x)$ along the whole cloud traverse is presented in Fig. 8. To facilitate comparison, the droplet concentration obtained from FFSSP measurements using the optimal estimator developed by Pawlowska and Brenguier (1997) is presented (denoted by points) as well. One can see a good agreement between the profiles of large-scale droplet concentration fluctuations calculated using the Fourier series and those retrieved with the optimal estimator. One can notice a good agreement between the two techniques down to very fine details, such as sharp peaks. Thus, the utilization of the Fourier series presents a rather effective method of retrieval of large-scale droplet concentration fluctuations in a cloud, down to the scale of a few meters.

One can see that the whole cloud traverse can be divided into three parts: 1) 0–120 m, where a substantial inhomogeneity of the large-scale concentration exists; 2) 120 m to about 250 m, where the large-scale droplet concentration is more homogeneous; and a third part, 3) from 250 m, with large fluctuations similar to the first. We attribute the droplet concentration fluctuations in the first and last segments to the influence of the surrounding air entrainment, decreasing further in the cloud. The second segment represents an adiabatic cloud core.

To compare the characteristics of small-scale fluctuations of droplet concentration within the homogeneous core with those over the whole cloud, the analysis has been conducted in both cases.

Figure 9 is similar to Fig. 8, with the exception that only the homogeneous cloud core is treated. Taking into account a comparably small length of the core, 50 harmonics were used for the description of large-scale droplet-concentration fluctuations. We can see again a good agreement of large-scale droplet concentration fluctuations calculated using the Fourier series with those revealed using the optimal estimator.

The results of calculations of the parameters of the small-scale structure in the whole cloud and in its adiabatic core are summarized in Table 2.

The estimated values of mean droplet concentration were 194.9 and 211.5 cm^{-3}, over the whole cloud and in the cloud core, respectively. Figure 10 shows the correlation function $\hat{B}^{\lambda'}(l)$ calculated according to (5.5) as a function of the distance between two points along the aircraft track over the whole cloud traverse. Fitting of the correlation function by an exponential function is shown in the figure as well. We can see that the approximation of the correlation function by an exponential function provides rather effective display of the behavior of the correlation function (similar to that was found in the tests). The correlation function in the homogeneous cloud core is quite similar to that over the whole cloud traverse. Despite substantial noise, the correlation function maximums are pronounced in both cases, indicating the existence of significant fluctuations of droplet concentration at the centimeter scale.

TABLE 2. Parameters of cloud structure revealed from in situ observations. Notations are as in Table 1.

	$\hat{\lambda}_{o,}$ cm^{-3}	$\hat{\sigma}_{\lambda'}$ (cm^{-3})	$\hat{\sigma}_{\lambda'}/\lambda_{o,}$ %	$\hat{l}_{\text{cor}}$ (cm)
The whole cloud traverse	194.87	60.59	31.09	0.48
The adiabatic cloud core	211.49	63.78	31.15	0.51

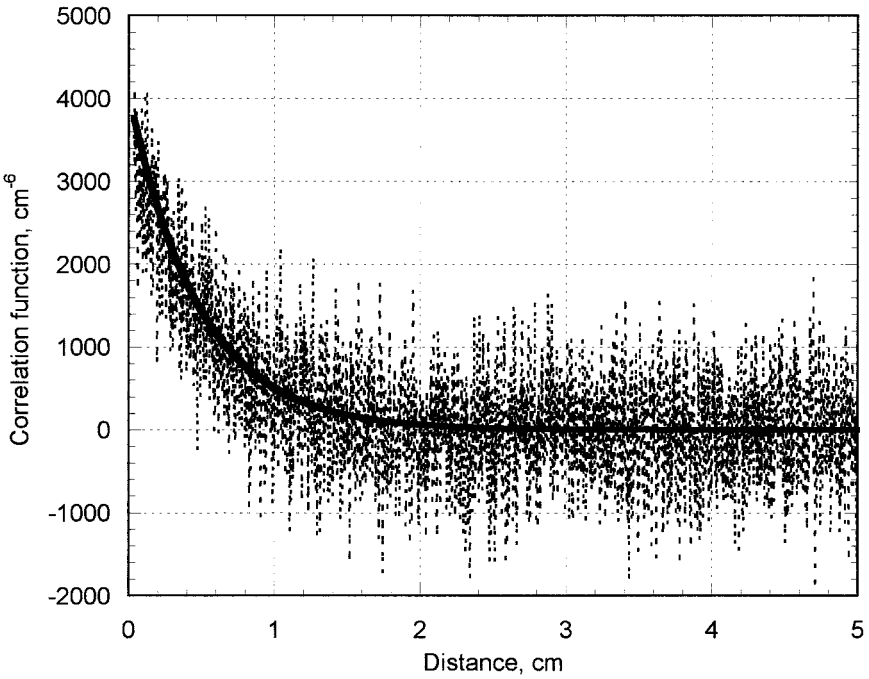

FIG. 10. The estimated correlation function $\hat{B}^{\lambda'}(l)$ calculated according to (5.5) as the function of the distance between two points in a cloud along the aircraft track over the whole cloud traverse. Despite the substantial noise, the correlation function maximum is pronounced, indicating the existence of significant small-scale concentration fluctuations. Exponential approximation of the correlation function is shown by solid line.

The rms amplitude of these fluctuations in the case study was estimated equal to 60.6 cm^{-3} (31.09% of the mean value) and 63.78 cm^{-3} (30.15%) over the whole cloud traverse and in the cloud core, respectively. The correlation length was 0.48 and 0.51 cm, respectively.

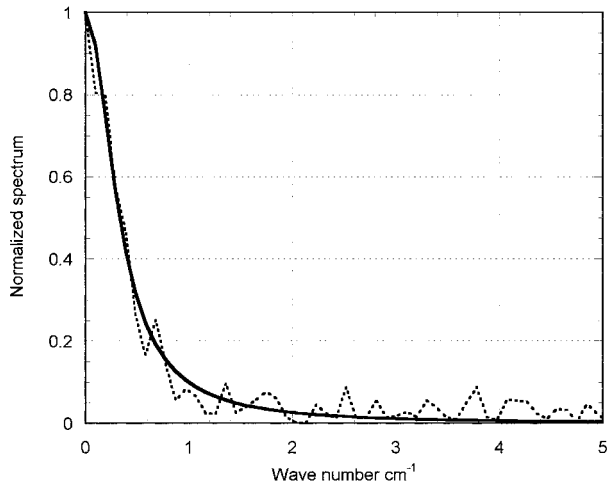

FIG. 11. The power spectrum corresponding to the correlation function, presented in Fig. 10 (the adiabatic core of the cloud). In the figure $\omega = 1/l$ is the wavenumber. The spectrum corresponding to the approximated correlation function is shown as well. About 80% of the energy of small-scale droplet concentration fluctuations is contained within the range 0.5–5 cm.

The Fourier transform of the correlation function yields the estimation of the energy spectrum $\hat{F}^{\lambda'}(\omega)$ of small-scale concentration fluctuations. Because of the similarity of the correlation functions, the power spectra calculated for the whole traverse and for the homogeneous core are also similar. That is why we present here (Fig. 11) only the spectrum related to the homogeneous core of the cloud. In the figure $\omega = I/l$ is the wavenumber.

To facilitate comparison, the theoretical spectrum (Feller 1966) of a signal with an exponential correlation function (corresponding to the solid line in Fig. 10) is presented in Fig. 11 as well. This spectrum can be written as

$$F(\omega) = \frac{2\gamma\sigma^2_{\lambda'}}{\gamma^2 + \omega^2}. \tag{7.1}$$

In the calculations, the maximum segment length was taken equal to 10 cm.

We can see that there are no droplet concentration fluctuations at scales smaller than about 0.5 cm (wavenumbers greater than 2) in the cloud. The power of the fluctuations increases rapidly with the increase of the length scale, and reaches significant values at a few centimeters.

At smaller scales the spectrum represents a noise cor-

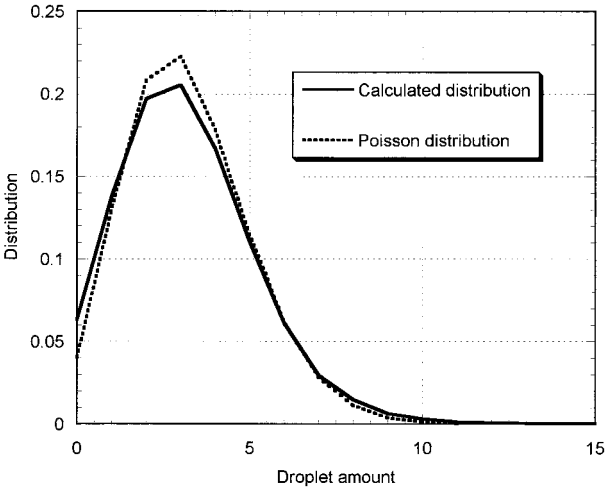

FIG. 12. Distributions of drop count in a 0.5-cm segment in the case study and the Poisson distribution with parameter calculated by averaging all over cloud traverse. One can see that in both cases the distributions are close.

responding to the noise in the correlation function. Note that Fig. 11 presents only the continuous part of the spectrum sketched in Fig. 2.

8. Discussion

Now we are going to discuss an apparent disagreement between the results of the present study and conclusions drawn by Chaumat and Brenguier (1998) based on the analysis of in situ observations.

In the latter study the conclusions about of the absence of centimeter-scale drop concentration fluctuations were based on a very little deviation of the drop count distribution within certain segments from the idealized Poisson distribution. The key point of the statistical analysis of the present study is that the information about small-scale drop concentration fluctuations is contained mainly in a 2D distribution and its moments (the correlation function and energy spectrum), and not in the shape of 1D distribution. With the purpose to demonstrate this point, we present Fig. 12, where drop count distributions are shown in a 0.5-cm segment in the present case study and in the case of the Poisson distribution with the parameter calculated by averaging all over the cloud traverse. We can see that the distributions are actually similar. Thus, the proximity of the distribution to the idealized Poisson distribution can hardly serve as evidence of either the presence or absence of small-scale droplet concentration fluctuations.

Note that this conclusion is not new. For example, Kostinski and Jameson (1997) and Kostinski and Jameson (1999) have used the correlation function of the number of raindrops within different unit volumes in relation with non-Poisson nature of precipitation fluctuations.

9. Conclusions

A method of analysis of droplet concentration fluctuations is developed utilizing the series of droplet arrival times measured by the FFSSP in a cloud. The main purpose of the analysis was to determine whether droplet concentration fluctuates at such small scales as a few centimeters or whether these fluctuations are negligible as compared with the mean concentration. In the analysis, the series of droplet arrival times is regarded as a generalized Poisson random process with time-dependent (or space dependent) parameters.

The method is based on the representation of droplet concentration in a cloud along an aircraft track as the sum of three terms: (i) average droplet concentration in a cloud, (ii) large-scale fluctuations of droplet concentrations coherent over the cloud length (they are described by the Fourier series), and (iii) small-scale noncoherent concentration fluctuations characterized by their energy parameters—the energy spectrum and cloud averaged correlation function.

The efficiency of the method as regards estimation of the amplitude and spatial characteristics of small-scale droplet concentration fluctuations, as well as calculation of the profile of the large-scale component of droplet concentration along the aircraft track, was tested using model simulated series of droplet arrival times. The parameters of the simulations were the root-mean-square value of the amplitude and the characteristic correlation length of droplet concentration fluctuations.

The results of the tests show that the method presented is efficient enough to retrieve both the amplitude and characteristic correlation length scale of small-scale fluctuations with a high accuracy beginning with scales as low as 2 mm. The amplitude was retrieved with an accuracy of about 5%. The method is able to reproduce profiles of ''large-scale'' concentration beginning with scales of a few meters.

The method was used for the analysis of a typical cumulus cloud section of 350 m length. The size distribution of cloud droplet radii in this case was centered at about 14 μm. The profiles of large-scale droplet concentration fluctuations along the aircraft track agree well with that obtained using the optimal estimator developed by Pawlowska and Brenguier (1997). Large-scale fluctuations of droplet concentration seem to be related to processes of entrainment and mixing in the vicinity of cloud boundaries.

The results of the calculations indicate the existence of pronounced small-scale droplet concentration fluctuations in the case study. Droplet concentration fluctuations with a length scales of one to a few centimeters were estimated to be about 30% over both the whole cloud and in the cloud core as compared with the mean values of droplet concentration. The power spectrum in Fig. 11 shows that fluctuations with spatial scales within the 0.5–5-cm range are responsible for more than 80% of the energy of small-scale concentration fluctuations.

This result suggests that droplets in clouds tend to cluster within centimeter-scale regions. In this particular case the analysis shows no significant droplet fluctuations at length scales below 0.5 cm.

The presence of small-scale droplet concentration fluctuations with actually the same spatial characteristics in the homogeneous core and over the whole cloud suggests that these fluctuations are caused by the process of a general nature, intrinsic to cloud physics.

As was mentioned above, droplet concentration fluctuations can be caused by turbulent velocity fluctuations obeying the $-5/3$ law. Let us evaluate the contribution of these drop concentration fluctuations to those on centimeter scale. Variation of ''large-scale'' drop concentration at scales of 100 m can be estimated as about 20% of mean concentration (Fig. 8). Using $-5/3$ law, one can evaluate the decrease in amplitude of fluctuations of the ''large-scale'' droplet concentration as proportional to $k^{-1/3}$, where k is a wavenumber. Thus, already at scales of 10 cm (within the inertial range) the amplitude falls to 2% of the mean fluctuation. At scales of 1 cm one can expect even lower-amplitude concentration fluctuations induced by turbulent velocity fluctuation and other large-scale mechanisms.

Hence, small-scale fluctuations, with amplitude of up to 30% of the mean concentration, revealed in the study cannot be induced by these large-scale effects.

Both spatial scales and amplitudes of small-scale droplet concentration, compare well with the theoretical evaluations given by Pinsky et al. (1999a), according to which droplet concentration fluctuations at centimeter scales are caused by the inertia of droplets moving within a turbulent flow. Thus, we interpret the results as evidence of turbulence effects on motion of cloud droplets due to their inertia.

To obtain more definite conclusions concerning the magnitudes of the centimeter-scale drop concentration fluctuations, as well as large-scale (over a few meters) droplet concentration fluctuations in different clouds, analysis of many samples of such data is required. According to Pinsky et al. (1999a), the divergence of the droplet velocity flux induced by droplet inertia increases with the increase in droplet mass and intensity of turbulence. We suppose that the rates of droplet concentration inhomogeneity are determined by these parameters, too. This statement can be verified in Part II using the data in several tens of cumulus clouds.

Acknowledgments. This study was supported by the Germany-Israel Science Foundation (Grant 0407-008.08/95) and the Israel Science Foundation administrated by the Israel Academy of Sciences and Humanities (Grant 143/99).

We are grateful to Dr. Jean-Louis Brenguier for providing the observed data, valuable discussion, and advice. The sections dedicated to the definition of drop concentration, as well as to testing of the algorithm proposed, were written in close collaboration with him. Dr. Jean-Louis Brenguier has encouraged us to provide better physical explanation of derivations and results. We are also grateful to Laure Chaumat for her help in the preparation of observed data.

APPENDIX A

The Relationship of the Poisson Parameter with the Components of Drop Concentration

Substituting (3.2), (3.3), and (3.6) into (2.7), we have

$$\begin{aligned}\frac{\overline{n}(x,\, l)}{S} &= \int_{x-l/2}^{x+l/2} \lambda(x')\, dx' \\ &= \lambda_o l + \sum_{k=1}^{\infty} a_k \int_{x-l/2}^{x+l/2} \cos k\omega_o x'\, dx' \\ &\quad + \sum_{k=1}^{\infty} b_k \int_{x-l/2}^{x+l/2} \sin k\omega_o x'\, dx' \\ &\quad + \frac{1}{2\pi} \int_{-\infty}^{+\infty} Z^{\lambda'}(\omega) \int_{x-l/2}^{x+l/2} e^{i\omega x'}\, dx'\, d\omega. \end{aligned} \tag{A1}$$

Integration in (A1) yields

$$\begin{aligned}\frac{1}{S}\overline{n}(x,\, l) &= \lambda_o l + \sum_{k=1}^{\infty} \frac{2a_k}{k\omega_o} \sin\frac{k\omega_o l}{2} \cos k\omega_o x \\ &\quad + \sum_{k=1}^{\infty} \frac{2b_k}{k\omega_o} \sin\frac{k\omega_o l}{2} \sin k\omega_o x \\ &\quad + \frac{1}{\pi} \int_{-\infty}^{+\infty} Z^{\lambda'}(\omega) e^{i\omega x} \sin\frac{\omega l}{2} \frac{d\omega}{\omega}. \end{aligned} \tag{A2}$$

Expression (A2) can be rewritten as

$$\begin{aligned}\overline{n}(x,\, l) &= \lambda_o S l \\ &\quad + \sum_{k=1}^{\infty} [A_k(l) \cos k\omega_o x + B_k(l) \sin k\omega_o x] \\ &\quad + \frac{S}{\pi} \int_{-\infty}^{+\infty} Z^{\lambda'}(\omega) e^{i\omega x} \sin\frac{\omega l}{2} \frac{d\omega}{\omega}. \end{aligned} \tag{A3}$$

Here

$$\begin{aligned} A_k(l) &= \frac{2a_k S}{k\omega_o} \sin\frac{k\omega_o l}{2}; \\ B_k(l) &= \frac{2b_k S}{k\omega_o} \sin\frac{k\omega_o l}{2}. \end{aligned} \tag{A4}$$

For small k and l when $k\omega_o l/2 < 0.1$,

$$A_k(l) \approx a_k Sl; \qquad B_k(l) = b_k Sl. \tag{A5}$$

Expression (A3) can be rewritten as

$$\overline{n}(x, l) = \overline{n_o} + \overline{n_1}(x, l) + \overline{n}'(x, l), \tag{A6}$$

where $\overline{n_o}$, $\overline{n_1}(x, l)$ and $\overline{n}'(x, l)$ are given by (4.2).

APPENDIX B

Averaging over the Whole Cloud

a. Cloud averaged Poisson distribution parameter in segment length l

Using (A3) one can write

$$\begin{aligned}\tilde{\overline{n}}(l) &= \frac{1}{L}\int_{-L/2}^{L/2} \overline{n}(x, l)\, dx \\ &= \lambda_o Sl + \frac{1}{L}\sum_{k=1}^{\infty} A_k(l)\int_{-L/2}^{L/2} \cos k\omega_o x\, dx \\ &\quad + \frac{1}{L}\sum_{k=1}^{\infty} B_k(l)\int_{-L/2}^{L/2} \sin k\omega_o x\, dx \\ &\quad + \frac{S}{\pi L}\int_{-\infty}^{+\infty} Z^{\lambda'}(\omega)\left(\int_{-L/2}^{L/2} e^{i\omega x}\, dx\right)\sin\frac{\omega l}{2}\frac{d\omega}{\omega},\end{aligned} \tag{B1}$$

where $\omega_o = 2\pi/L$. The second and the third terms on the right side of (B1) are equal to zero because the integrals in the terms diminish.

Integration in the last term yields

$$\begin{aligned}\tilde{\overline{n}}(l) &= \lambda_o Sl \\ &\quad + \frac{2}{\pi L}\int_{-\infty}^{+\infty} Z^{\lambda'}(\omega)\frac{e^{i\omega L/2} - e^{-i\omega L/2}}{2i}\sin\frac{\omega l}{2}\frac{d\omega}{\omega^2} \\ &= \lambda_o Sl + \frac{S}{\pi}\int_{-\infty}^{+\infty} Z^{\lambda'}(\omega)\frac{\sin\dfrac{\omega L}{2}}{\dfrac{\omega L}{2}}\sin\frac{\omega l}{2}\frac{d\omega}{\omega}.\end{aligned} \tag{B2}$$

Assuming the cloud length L is much larger than the maximum scale of small-scale concentration inhomogeneities, we can use the limit representation of the delta function $\delta(x)$ (see Korn and Korn 1968):

$$\lim_{a\to\infty} = \frac{a}{\pi}\frac{\sin ax}{ax} = \delta(x),$$

Replacing $[\sin(\omega L/2)/(\omega L/2)]$ by the delta function in expression (B2), we have

$$\frac{\sin\dfrac{\omega L}{2}}{\dfrac{\omega L}{2}} = \frac{2\pi}{L}\delta(\omega). \tag{B3}$$

Substitution of (B3) into (B2) yields

$$\tilde{\overline{n}}(l) = \lambda_o Sl + \frac{2S}{L}\int_{-\infty}^{+\infty} Z^{\lambda'}(\omega)\delta(\omega)\sin\frac{\omega l}{2}\frac{d\omega}{\omega}. \tag{B4}$$

Convolution with the delta function in (B4) leads to the following expression:

$$\tilde{\overline{n}}(l) = \lambda_o Sl + \frac{Sl}{L}Z^{\lambda'}(0). \tag{B5}$$

The last term contains averaging of drop fluctuation over the whole cloud, and according to the definition it is equal to zero. Last, we have

$$\overline{\tilde{n}}(l) = \lambda_o Sl, \tag{B6}$$

Strictly speaking, equality (B6) is valid with the precision of $O(l_m/L)$, where l_m is the maximum length scale of small-scale concentration inhomogeneities.

b. Additional cloud averaged values $\tilde{n}_{Ak}(l)$ and $\tilde{n}_{Bk}(l)$

Using (A3) one can write

$$\begin{aligned}\tilde{n}_{Ak}(l) &= \frac{2}{L}\int_{-L/2}^{L/2} \overline{n}(x, l)\cos k\omega_o x\, dx = \lambda_o Sl\frac{2}{L}\int_{-L/2}^{L/2}\cos k\omega_o x\, dx \\ &\quad + \frac{2}{L}\sum_{j=1}^{\infty} A_j(l)\int_{-L/2}^{L/2}\cos j\omega_o x\cos k\omega_o x\, dx + \frac{2}{L}\sum_{j=1}^{\infty} B_j(l)\int_{-L/2}^{L/2}\sin j\omega_o x\cos k\omega_o x\, dx \\ &\quad + \frac{S}{\pi}\frac{2}{L}\int_{-\infty}^{+\infty} Z^{\lambda'}(\omega)\left(\int_{-L/2}^{L/2}\cos k\omega_o x\, e^{i\omega x}\, dx\right)\sin\frac{\omega l}{2}\frac{d\omega}{\omega}.\end{aligned} \tag{B7}$$

The first term on the right side is equal to zero. The second term is not equal to zero only when $k = j$ because of the orthogonality of functions $\cos j\omega_o x$ and $\cos k\omega_o x$.

The third term is equal to zero because of the orthogonality of functions $\sin j\omega_o x$ and $\cos k\omega_o x$. The integral with respect to x in the last term should be small

because of the noncoherence of terms $\cos k\omega_o x$ and $e^{i\omega x}$. Thus, (B7) can be rewritten in the form

$$\tilde{n}_{Ak}(l) = \frac{2}{L} A_k(l) \int_{-L/2}^{L/2} \cos^2 k\omega_o x \, dx = A_k(l). \quad \text{(B8)}$$

Averaged values $\tilde{n}_{Bk}(l)$ are calculated in a similar way:

$$\tilde{n}_{Bk}(l) = B_k(l), \quad \text{(B9)}$$

where $k = 1, 2 \ldots$.

c. Cloud averaged square of the Poisson parameter distribution in length segment l

According to the definition,

$$\tilde{\overline{n}}^2(l) = \frac{1}{L} \int_{-L/2}^{L/2} [\overline{n}(x, l)]^2 \, dx. \quad \text{(B10)}$$

Substitution of (A6) into (B10) leads to the following expression:

$$\tilde{\overline{n}}^2(l) = \frac{1}{L} \int_{-L/2}^{L/2} [\overline{n}_o^2 + \overline{n}_1^2(x, l) + \overline{n}_1'^2(x, l) + 2\overline{n}_o\overline{n}_1(x, l) + 2\overline{n}_o\overline{n'}(x, l) + 2\overline{n}_1(x, l)\overline{n}'(x, l)] \, dx \quad \text{(B11)}$$

The integral of the first terms is equal to $(\lambda_o Sl)^2$. Because of the noncoherence of the terms and because of the orthogonality of functions $\sin j\omega_o x$ and $\cos k\omega_o x$, integrals of the 4th, 5th, and 6th terms are equal to zero. Thus,

$$\tilde{\overline{n}}^2(l) = (\lambda_o Sl)^2 + \frac{1}{L} \int_{-L/2}^{L/2} [\overline{n}_1(x, l)]^2 \, dx + \frac{1}{L} \int_{-L/2}^{L/2} [\overline{n}'(x, l)]^2 \, dx. \quad \text{(B12)}$$

Substituting corresponding expressions for $\overline{n}_1(x, l)$ and $\overline{n}'(x, l)$ from (4.2) we have

$$\tilde{\overline{n}}^2(l) = (\lambda_o Sl)^2 + \frac{1}{L} \int_{-L/2}^{L/2} \left[\sum_{k=1}^{\infty} A_k(l) \cos k\omega_o x + \sum_{k=1}^{\infty} B_k(l) \sin k\omega_o x \right]^2 dx + \frac{1}{L} \frac{S^2}{\pi^2} \int_{-L/2}^{L/2} \int_{-\infty}^{\infty} \int_{-\infty}^{\infty} Z^{\lambda'*}(\omega') Z^{\lambda'}(\omega'') e^{i\omega'' x} e^{-i\omega' x} \sin\frac{\omega' l}{2} \sin\frac{\omega'' l}{2} \frac{d\omega'}{\omega'} \frac{d\omega''}{\omega''} \, dx. \quad \text{(B13)}$$

Here symbol * denotes a complex conjunctive value. Taking into account the orthogonality of functions $\sin k\omega_o x$ and $\cos j\omega_o x$ in the second term, changing the sequence of integration in the last term (B13), and carrying out the integration with respect to x, we obtain

$$\begin{aligned} \tilde{\overline{n}}^2(l) &= (\lambda_o Sl)^2 + \frac{1}{L} \int_{-L/2}^{L/2} \left[\sum_{k=1}^{\infty} A_k^2(l) \cos^2 k\omega_o x + \sum_{k=1}^{\infty} B_k^2(l) \sin^2 k\omega_o x \right] dx \\ &\quad + \frac{S^2}{\pi^2 L} \int_{-\infty}^{\infty} \int_{-\infty}^{\infty} Z^{\lambda'*}(\omega') Z^{\lambda'}(\omega'') \left[\int_{-L/2}^{L/2} e^{i(\omega''-\omega')x} \, dx \right] \sin\frac{\omega' l}{2} \sin\frac{\omega'' l}{2} \frac{d\omega'}{\omega'} \frac{d\omega''}{\omega''} \\ &= (\lambda_o Sl)^2 + \frac{1}{2} \sum_{k=1}^{\infty} [A_k^2(l) + B_k^2(l)] \\ &\quad + \frac{S^2}{\pi^2 L} \int_{-\infty}^{\infty} \int_{-\infty}^{\infty} Z^{\lambda'*}(\omega') Z^{\lambda'}(\omega'') \frac{\sin[(\omega'' - \omega')L/2]}{(\omega'' - \omega')} \sin\frac{\omega' l}{2} \sin\frac{\omega'' l}{2} \frac{d\omega'}{\omega'} \frac{d\omega''}{\omega''}. \end{aligned} \quad \text{(B14)}$$

Using the limit approximation of the δ-function, which is valid when the cloud length is significantly greater

than the maximum length of small-scale drop concentration inhomogeneities, we have

$$\frac{\sin[(\omega'' - \omega')L/2]}{(\omega'' - \omega')} \to \frac{2\pi}{L}\delta(\omega'' - \omega'). \quad \text{(B15)}$$

Substituting (B15) into (B14), introducing new variables of integration: $\omega = \omega''$ and $\Omega = \omega'' - \omega'$, and carrying out the integration with respect to Ω, the last integral in (B14) can be rewritten as:

$$\frac{2S^2}{\pi L}\int_{-\infty}^{\infty} |Z^{\lambda'}(\omega)|^2 \sin^2\frac{\omega l}{2}\frac{d\omega}{\omega^2}.$$

Using the definition of the energy spectrum $F^{\lambda'}(\omega) = (2/L)|Z^{\lambda'}(\omega)|^2$, one can write (B14) as

$$\tilde{\bar{n}}^2(l) = (\lambda_o Sl)^2 + \frac{1}{2}\sum_{k=1}^{\infty}[A_k^2(l) + B_k^2(l)] + \frac{S^2}{\pi}\int_{-\infty}^{\infty} F^{\lambda'}(\omega)\sin^2\frac{\omega l}{2}\frac{d\omega}{\omega^2}. \quad \text{(B16)}$$

d. Transfer to the correlation function

With (A5), expression (B16) yields

$$\tilde{\bar{n}}^2(l) = (\lambda_o Sl)^2 + \frac{(Sl)^2}{2}\sum_{k=1}^{\infty}(a_k^2 + b_k^2) + \frac{S^2}{\pi}\int_{-\infty}^{\infty} F^{\lambda'}(\omega)\sin^2\frac{\omega l}{2}\frac{d\omega}{\omega^2}. \quad \text{(B17)}$$

Double differentiation of (B17) with respect to l yields

$$\frac{d^2\tilde{\bar{n}}^2(l)}{dl^2} = 2(\lambda_o S)^2 + S^2\sum_{k=1}^{\infty}(a_k^2 + b_k^2) + \frac{S^2}{2\pi}\int_{-\infty}^{\infty} F^{\lambda'}(\omega)\cos\omega l\, d\omega. \quad \text{(B18)}$$

The correlation function and the energetic spectrum are related through the Fourier transform (3.11)

$$B^{\lambda'}(l) = \frac{1}{4\pi}\int_{-\infty}^{+\infty} F^{\lambda'}(\omega)\exp(i\omega l)\, d\omega = \frac{1}{4\pi}\int_{-\infty}^{+\infty} F^{\lambda'}(\omega)\cos(\omega l)\, d\omega.$$

Using this latter expression, (B18) can be finally rewritten as

$$\frac{1}{2S^2}\frac{d^2\tilde{\bar{n}}^2(l)}{dl^2} = \lambda_o^2 + \frac{1}{2}\sum_{k=1}^{\infty}(a_k^2 + b_k^2) + B^{\lambda'}(l). \quad \text{(B19)}$$

APPENDIX C

The Bias of Estimations

Hereinafter, we will assume $l \ll L$. It means that the values averaged over the whole cloud length L are equal to the values averaged over segment $L - l$ with the precision of $O(l/L)$:

$$\frac{1}{L}\int_{-L/2}^{L/2} A\, dx = \frac{1}{L}\int_{-(L-l)/2}^{(L+l)/2} A\, dx + O(l/L).$$

Thus, the estimation bias will be evaluated with the precision $O(l/L)$. This precision is high enough: even for small clouds the ratio l/L is of the order 10^{-4}.

a. Mean concentration

From (5.1) we have

$$\langle\hat{\lambda}_o\rangle = \frac{1}{Sl}\cdot\frac{1}{L-l}\int_{-(L-l)/2}^{(L-l)/2}\langle n(x, l)\rangle\, dx.$$

Calculating the mathematical expectation of both sides of (5.1) one can obtain

$$\langle\hat{\lambda}_o\rangle = \frac{1}{Sl}\cdot\frac{1}{L-l}\int_{-(L-l)/2}^{(L-l)/2}\overline{n(x, l)}\, dx \approx \frac{1}{Sl}\cdot\frac{1}{L}\int_{-L/2}^{L/2}\overline{n(x, l)}\, dx.$$

From (4.5) we can see that

$$\langle\hat{\lambda}_o\rangle = \frac{1}{Sl}\tilde{\bar{n}}(l),$$

and from (4.7), we conclude that

$$\langle\hat{\lambda}_o\rangle = \lambda_o. \quad \text{(C1)}$$

Equality (C1) means that the estimation $\hat{\lambda}_o$ has no bias.

b. The Fourier series coefficients

From (5.2) we have

$$\langle\hat{a}_k\rangle = \frac{1}{Sl}\frac{2}{L-l}\int_{-(L-l)/2}^{(L-l)/2}\langle n(x, l)\rangle\cos(k\omega_o x)\, dx = \frac{1}{Sl}\frac{2}{L-l}\int_{-(L-l)/2}^{(L-l)/2}\overline{n}(x, l)\cos(k\omega_o x)\, dx \approx \frac{1}{Sl}\frac{2}{L}\int_{-L/2}^{L/2}\overline{n}(x, l)\cos(k\omega_o x)\, dx.$$

From (4.8) we have $\langle\hat{a}_k\rangle = (1/Sl)\tilde{n}_{A_k}(l)$ and from (4.9) we conclude that

$$\langle\hat{a}_k\rangle = a_k. \quad \text{(C2)}$$

Similarly:

$$\langle\hat{b}_k\rangle = b_k. \quad \text{(C3)}$$

c. Correlation function

Equation (5.3) yields

$$\left\langle\widehat{\widetilde{\bar{n}}^2}(l)\right\rangle = \frac{1}{L-l}\int_{-(L-l)/2}^{(L-l)/2}\langle n^2(x, l)\rangle\, dx.$$

Using (2.8) we obtain

$$\left\langle \widehat{\overline{n}^2}(l) \right\rangle = \frac{1}{L-l} \int_{-(L-l)/2}^{(L-l)/2} [\overline{n}^2(x, l) + \overline{n}(x, l)]\, dx \approx \frac{1}{L} \int_{-L/2}^{L/2} [\overline{n}^2(x, l) + \overline{n}(x, l)]\, dx.$$

Using (4.5)–(4.7) and (4.10)–(4.13), the mathematical expectation of $\tilde{n}^2$ can be written as

$$\left\langle \widehat{\overline{n}^2}(l) \right\rangle = \widetilde{\overline{n}_o^2}(l) + \widetilde{\overline{n}_1^2}(l) + \widetilde{\overline{n'^2}}(l) + \tilde{\bar{n}}(l) = (\lambda_o Sl)^2 + \frac{(Sl)^2}{2} \sum_{k=1}^{\infty} (a_k^2 + b_k^2) + \frac{S^2}{\pi} \int_{-\infty}^{+\infty} F^{\lambda'}(\omega) \sin^2\left(\frac{\omega l}{2}\right) \frac{d\omega}{\omega^2} + \lambda_o Sl. \quad \text{(C4)}$$

The last term on the right side of expression (C4) determines the bias of the mean square value of cloud averaged drop concentration. This bias is caused by ''natural'' Poisson fluctuations of drop counts. However, the bias can be eliminated by double differentiation of (C4). Despite all this, the term is the main source of random errors, at least, for small l. Taking the derivative of (C4) twice with respect to l and comparing the result with (4.14), we obtain

$$\langle \hat{B}^{\lambda'}(l) \rangle = B^{\lambda'}(l). \quad \text{(C5)}$$

APPENDIX D

Possible Effects of Centimeter-Scale Droplet Concentration Inhomogeneities on Droplet Spectrum Formation

A natural question arises: what could be the role of these centimeter-scale droplet concentration fluctuations in droplet spectrum formation? Two mechanisms related to effects on drop collisions and effects on differential growth by diffusion can be assumed.

The collision rate of droplets is affected by mechanisms related to inhomogeneous droplet concentration and to turbulent effects on the collision kernel.

Let us evaluate a potential effect of the droplet concentration fluctuations basing on both theoretical results by Pinsky et al. (1999a) and on the statistical analysis of the present study. As follows from the stochastic kinetic equation of collisions, the growth rate (frequency of drop collisions) is proportional to the multiplication of their concentrations n_1 and n_2. Thus, in case of positive fluctuations of drop concentration of 30%–40% of the mean value, the frequency of collisions increases in the areas of enhanced droplet concentration by a factor of 1.7 to 2. To evaluate the effect of these ''subgrid'' fluctuations of drop concentration on the collision rate averaged over large volumes of 10^7–10^{10} m^3, typical of cloud model resolution, we have to evaluate the mean value of the product $n_1 n_2$. One can write $\langle n_1 n_2 \rangle = \langle n_1 \rangle \langle n_2 \rangle + R\sigma_1\sigma_2$, where symbol $\langle\ \rangle$ denotes averaging over a certain volume on the order of 10^7–10^{10} m^3, σ_1 and σ_2 are the rms values of drop concentration fluctuations, and R is the correlation coefficient. In cloud models based on the stochastic kinetic equations of collisions the value $\langle n_1 \rangle \langle n_2 \rangle$ is usually used. We can see that in case of positive correlation between drop concentration fluctuations, concentration inhomogeneity accelerates the collision process. This fact was discussed by Voloshuk (1984), Kasper (1984), and Pinsky and Khain (1997). According to Khain and Pinsky (1997) and Pinsky et al (1999a), small droplets with the radii ranging from 5 to about 15 μm tend to concentrate in the same regions of a turbulent flow, so that the coefficient of correlation R is close to 1. Thus, from the latter formula, the mean drop growth rate due to small droplet concentration (the autoconversion rate) increases by 10% to 15%. Note, that droplet flux velocity divergence is proportional to the square of the drop radii (Pinsky et al 1999a). Thus, one can expect that the rms of concentration fluctuations of 20-μm-radii droplets is significantly higher than the rms of 10-μm-radii droplets. Hence, the contribution of small-scale drop concentration fluctuations to the frequency of collisions can be as important as that of mean values.

The problem of collisions of 100-μm-radii drops and small droplets requires a special analysis. Pinsky and Khain (1997) showed that the maximum of relative fluctuations of concentration took place for droplets of radii about 100 μm. Raindrops significantly larger than 100 μm in radii do not respond to turbulent shears. Characteristic scales of small 100–200 μm-radii raindrop clusters (caused by their inertia) range from a few meters to tens of meters. Pinsky and Khain (1997) assumed the existence of a ''self-concentration'' process of droplet collisions: larger cloud droplets being formed, tend to concentrate in certain volumes, where their concentration turns out to be much higher than the averaged concentration of such drops. The increase in the concentration of these droplets increases the probability of their collisions with the formation of even larger droplets. These droplets, in their turn, tend to concentrate with even higher rate, and so on. The main idea of the assumption is that fast droplet spectrum broadening with formation of rain drops takes place in regions, where the concentration of larger cloud droplets is much higher than the mean (averaged) concentration of such drops. In other areas the collisions of larger cloud droplets are too rare to form rain drops. This process was simulated by Pinsky and Khain (1997) using a simple model. A faster broadening of the ''mean'' spectrum was obtained, as compared to that of homogeneous droplet concentration.

Clustering of raindrops and related fluctuations of precipitation and their possible relation to turbulence are discussed by Kostinski and Jameson (1997, 2000). Further investigations are required to investigate the process.

The process of self-concentration can be very important in case of ice particles. It is known that ice particles' concentration is highly inhomogeneous. High ice concentrations are observed in areas of enhanced turbulence. The process of collisions of drop and ice particles fields is a complicated problem. Note, however, that the simple evaluations presented above indicate the significance of the effect of hydrometeors' concentration inhomogeneity on cloud evolution.

The formation of centimeter-scale droplet concentration inhomogeneities means the formation of additional inertial induced component of drop–drop relative velocity in addition to that induced by gravity. Pinsky et al. (1999b, 2000) show that even small changes in the relative velocities between droplets can lead to a significant increase in the collision efficiency of droplets and to the acceleration of the process of collisions.

The second mechanism through which centimeter-scale concentration fluctuations could influence droplet spectrum broadening is the dependence of supersaturation on the droplet concentration. There were several attempts to simulate this effect (Shaw et al. 1998; Vallencourt et al. 1998; Pinsky et al. 1999a). The conclusions drawn in these studies were quite contradictory.

Note that all attempts are mainly of heuristic nature and the problem requires further investigations. To simulate properly the effects of small-scale fluctuations on droplet growth by diffusion, we need to know 1) spatial scales and amplitudes of the fluctuations and 2) lifetime of these fluctuations.

It is obvious that the results of evaluation should be crucially dependent not only on the amplitude, but also on of the time characteristics of the centimeter-scale droplet concentration fluctuations (e.g., Grabowski and Vaillancourt 1999). Pinsky et al. (1999a) assumed the characteristic time of such drop concentration fluctuations to be equal to the characteristic time of air turbulent vortices of similar size. It means that the characteristic lifetime of centimeter-scale drop concentration inhomogeneities was assumed to be about 0.2 s. Droplets ascending in clouds experience both positive and negative deviations of supersaturation. In case such small lifetime is assumed, different droplets reaching the same level within a cloud experience actually the same history of supersaturation, so that droplet spectrum broadening turns out to be negligibly small. On the other hand, Shaw et al. (1998) assumed the lifetimes of inch clouds to be 10 times as long as the lifetime of an air vortex of similar size. As a result, a pronounced broadening of droplet spectrum was found.

The solution of the problem requires much better understanding of the turbulence structure in clouds at high Reynolds numbers, as well as of the statistical time characteristics of inertial droplets motion within a turbulent flow. The presented method gives valuable information concerning spatial and amplitude characteristics of centimeter-scale droplet concentration fluctuation but provides no information about the timescales of concentration inhomogeneities.

REFERENCES

Abramovitz, I., and I. A. Stegan, 1964: *Handbook of Mathematical Functions.* Applied Mathematics Series, Vol. 55, National Bureau of Standards, 1060 pp.

Baker, B. A., 1992: Turbulent entrainment and mixing in clouds: A new observational approach. *J. Atmos. Sci.,* **49,** 387–404.

Baumgardner, D., 1986: A new technique for the study of cloud microstructure. *J. Atmos. Oceanic Technol.,* **3,** 340–343.

Brenguier, J.-L., D. Baumgardner, and B. Baker, 1994: A review and discussion of processing algorithms for FSSP concentration measurements. *J. Atmos. Oceanic Technol.,* **11,** 1409–1414.

——, T. Bourianne, A. Coelho, J. Isbert, R. Peytavi, D. Trevarin, and P. Wechsler, 1998: Improvements of droplet size distribution measurements with the Fast FSSP. *J. Atmos. Oceanic Technol.,* **15,** 1077–1090.

Chaumat, L., and J.-L. Brenguier, 1998: Droplet spectra broadening and concentration inhomogeneities. Preprints, *Conf. on Cloud Physics and 14th Conf. on Planned and Inadvertent Weather Modification,* Everett, WA, Amer. Meteor. Soc., 514–517.

Cooper, W. A., 1989: Effects of variable droplet growth histories on droplet distributions. Part 1: Theory. *J. Atmos. Sci.,* **46,** 1301–1311.

Elperin, T., N. Kleeorin, and I. Rogachevskii, 1996: Self-excitation of fluctuations of inertial particles concentration in turbulent flow. *Phys. Rev. Lett.,* **77,** 5373–5376.

Feller, W., 1966: *An Introduction to Probability Theory and Its Applications.* Vol. 2. John Wiley and Sons, 626 pp.

Fessler, J. R., J. D. Kulick, and J. K. Eaton, 1994: Preferential concentration of heavy particles in a turbulent channel flow. *Phys. Fluids,* **6,** 3742–3749.

Grabowski, W. W., and T. L. Clark, 1991: Cloud environment interface instability-rising thermal calculations in two spatial dimensions. *J. Atmos. Sci.,* **48,** 527–546.

——, and P. Vaillancourt, 1999: Comments on the ''Preferential concentration of cloud droplets by turbulence: Effects on the early evolution of cumulus cloud droplet spectra.'' *J. Atmos. Sci.,* **56,** 1433–1436.

Kasper, G., 1984: On the coagulation rate with spatially inhomogeneous particle concentration. *J. Colloid Interface Sci.,* **102,** 560–562.

Korn, G. A., and T. M. Korn, 1968: *Mathematical Handbook for Scientists and Engineers.* McGraw-Hill, 831 pp.

Korolev, A. V., and I. P. Mazin, 1993: Zones of increased and decreased droplet concentration in stratiform clouds. *J. Appl. Meteor.,* **32,** 760–773.

Kostinski, A. B., and A. R. Jameson, 1997: Fluctuation properties of precipitation. Part I: On deviations of single-size drop counts from the Poisson distribution. *J. Atmos. Sci.,* **54,** 2174–2186.

——, and ——, 1999: Fluctuation properties of precipitation. Part III: On the ubiquity and emergence of the exponential drop size spectra. *J. Atmos. Sci.,* **56,** 111–121.

——, and ——, 2000: On the spatial distribution of cloud particles. *J. Atmos. Sci.,* **57,** 901–915.

Maxey, M. R., 1987: The gravitational settling of aerosol particles in homogeneous turbulence and random flow fields. *J. Fluid. Mech.,* **174,** 441–465.

Monin, A. S., and A. M. Yaglom, 1975: *Statistical Fluid Mechanics.* Vol. 2, *Mechanics of Turbulence,* MIT Press, 874 pp.

Pawlowska, H., and J.-L. Brenguier, 1997: Optimal nonlinear estimation for cloud particle measurements. *J. Atmos. Oceanic Technol.,* **14,** 88–104.

Pinsky, M. B., and A. P. Khain, 1996: Simulations of drops' fall in a homogeneous isotropic turbulence flow. *Atmos. Res.,* **40,** 223–259.

——, and ——, 1997: Formation of inhomogeneity in drop concen-

tration induced by drop inertia and their contribution to the drop spectrum broadening. *Quart. J. Roy. Meteor. Soc.,* **123,** 165–186.

——, ——, and Z. Levin, 1999a: The role of the inertia of cloud drops in the evolution of the drop size spectra during drop growth by diffusion. *Quart. J. Roy. Meteor. Soc.,* **125,** 553–581.

——, ——, and M. Shapiro, 1999b: Collisions of small drops in a turbulent flow. Part I: Collision efficiency: Problem formulation and preliminary results. *J. Atmos. Sci.,* **56,** 2585–2600.

——, ——, and ——, 2000: Stochastic effects of cloud droplet hydrodynamic interaction in a turbulent flow. *Atmos. Res.,* **53,** 131–169.

Shaw, R., W. C. Reade, L. R. Collins, and J. Verlinde, 1998: Preferential concentration of cloud droplets by turbulence: Effects on the early evolution of cumulus cloud droplet spectra. *J. Atmos. Sci.,* **55,** 1965–1976.

Vailliancourt, P. A., M. K. Yau, and W. Grabowski, 1998: Microphysic approach to condensational growth of cloud droplets. Preprints, *Conf. on Cloud Physics and 14th Conf. on Planned and Inadvertent Weather Modification,* Everett, WA, Amer. Meteor. Soc., 546–549.

Vohl, O., S. K. Mitra, S. C. Wurzler, and H. R. Pruppacher, 1999: A wind tunnel study of the effects of turbulence on the growth of cloud drops by collision and coalescence. *J. Atmos. Sci.,* **56,** 4088–4099.

Voloshuk, V. M., 1984: *The Kinetic Theory of Coagulation.* Gidrometizdat, 283 pp.

Wang, L.-P., and M. R. Maxey, 1993: Settling velocity and concentration distribution of heavy particles in homogeneous isotropic turbulence. *J. Fluid Mech.,* **256,** 27–68.

Warhaft, Z., 2000: Passive scalars in turbulent flows. *Annu. Rev. Fluid Mech.,* **32,** 203–240.

Yaglom, A. M., 1987: *Correlation Theory of Stationary and Related Random Functions.* Vols. 1 and 2. Springer, 726 pp.

Zhou, Y., A. S. Wexler, and L.-P. Wang, 1998: On the collision rate of small particles in isotropic turbulence. II. Finite inertia case. *Phys. Fluid,* **10,** 1206–1216.